MARMARA UNIVERSITY
FACULTY OF ENGINEERING

MECHANICAL CHARACTERIZATION OF CHITOSAN BASED WOUND DRESSING MATERIALS REINFORCED WITH NANOPARTICLES

Barkın AYDIN, Nihat AROL, Nimet BURAK

GRADUATION PROJECT REPORT

Department of Mechanical Engineering

Supervisor

Asst. Prof. Dr. Aybala YILDIRIM

ISTANBUL, 2023

MARMARA UNIVERSITY
FACULTY OF ENGINEERING

MECHANICAL CHARACTERIZATION OF CHITOSAN BASED WOUND DRESSING MATERIALS REINFORCED WITH NANOPARTICLES

By

Barkın AYDIN, Nihat AROL, Nimet BURAK

June 8, 2023, Istanbul

SUBMITTED TO THE DEPARTMENT OF MECHANICAL ENGINEERING
I N PARTIAL FULFILLMENT OF THE REQUIREMENTS FOR THE DEGREE

OF

BACHELOR OF SCIENCE

AT

MARMARA UNIVERSITY

Barkın Aydın Nihat Arol Nimet Burak

Signature of Author(s) ....

Department of Mechanical Engineering

Certified By .....

Project Supervisor, Department of Mechanical Engineering

Accepted By.....

Head of the Department of Mechanical Engineering

ACKNOWLEDGEMENT

First of all, we would like to thank our supervisor Asst. Prof. Dr. Aybala YILDIRIM, for the valuable guidance and advice on preparing this thesis and giving us moral and material support.

Also, we would like to thank Assoc. Prof. Muhammet CEYLAN for allowing us to work in his lab and use his equipment. Also, we would like to thank Dr. Serkan ÖĞÜT for his valuable time he shares with us during the tensile testing.

June 2023

Barkın AYDIN

Nihat AROL

Nimet BURAK

CONTENTS

ABSTRACT

The skin is a covering system organ that covers the human body. Since it is in the outermost layer, it is very vulnerable to injuries and deformations. Wound dressing materials play an important role in the treatment of these wounds. For these materials to heal wounds, their properties must be at an optimum level. Studies and developments are continuing to ensure this.

In this project, this wound dressing material, which plays an important role in our lives, was examined in 2 parts. Firstly, nanofiber mats containing polycaprolactone, boric acid, and zinc oxide, which can accelerate healing with their hydrophobic, antibacterial, and high mechanical properties, and secondly, hydrogels with polyvinyl alcohol and chitosan basic content, which can accelerate healing with their high moisture retention, biocompatibility, and antibacterial properties.

The aim of this project is to examine the contribution of boric acid, zinc oxide, polycaprolactone, polyvinyl alcohol, and chitosan, which are used in different ratios in the mentioned nanofiber mats and hydrogels, to the mechanical properties of the wound dressing material. To examine these effects, tensile test, compression test, contact angle test, and swelling ratio tests were performed.

SYMBOLS

mm	: Millimeter
mL	: Milliliter
g	: Gram
g/cm^3	: Gram per cubic centimeter (Density)
kV	**:** Kilovolts
γ	**:** Interface Energy
θ_c	**:** Contact Angle
F_t	: Tensile Force
w	: Width
t	: Thickness
A	: Cross-sectional Area
σ_t	: Tensile Stress
σ_c	: Compressive Stress
$\dot{\varepsilon}$	: Strain Rate
ε	: Strain
E	: Elastic Modulus
L	: Final Length
L_0	: Initial Length
MPa	: Megapascal
N	: Newton
W_D	: Weight of the specimen before swelling
W_S	: Weight of the specimen after swelling

ABREVIATIONS

BA : Boric Acid

CS : Chitosan

FTIR **:** Fourier Transform Infrared Spectroscopy

GA : Glutaraldehyde

PCL **:** Polycaprolactone

PVA **:** Polyvinyl Alcohol

SR **:** Swelling Ratio

ZnO : Zinc Oxide

LIST OF FIGURES

LIST OF TABLES

1) INTRODUCTION

1.1 Wounds and Wound Dressings

The skin acts as the first protective barrier on the outer surface of the human body, also safeguarding the internal organs against potential harm from the environment [1]. As a result, it is common for the skin to encounter different types of wounds, ranging from chronic wounds to those that are more easily healed [2]. Wounds are injuries that result in the breaking of the skin or other tissues in the body. They cover cuts, scrapes, scratches, and instances where the skin is punctured. While accidents are a common cause of wounds, wounds can also arise from surgical procedures [3, 4].

Wound healing is a complex and dynamic biological process that is done by replacing the damaged tissue with a newly produced one. It has four consecutive phases, which are hemostasis, inflammation, proliferation, and remodeling [5]. A rapid healing with minimal scarring is desired in the usage of wound dressing. Wound dressing developers have focused on safeguarding and providing coverage to wounds to prevent microbial infections for an extended period of time. To fulfill this desire the used material in the wound dressing must be absorbent for excessive exudates, permeable for gas exchange and mechanically strong for protecting the wound from any sort of damage that may cause from outside. Also, it should keep the wound bed moist [6,7]. It is also expected to be easily removable, replaceable, and affordable for commercial usage purposes [8]. There are many types of modern dressings, such as hydrogels, hydrocolloids, alginates, foams, and nanofiber films [9]. Due to their attractive properties, nanofiber mats and hydrogels are desirable materials in biomedical applications including wound dressing [10,11].

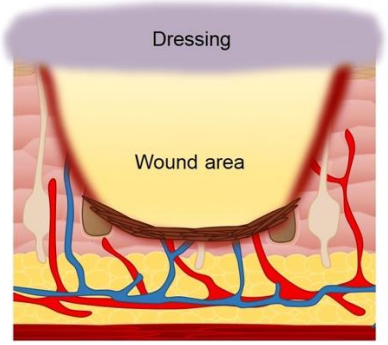

Figure 1: Wound dressing schematic [12].

Figure 2: Different types of dressings [9].

As mentioned earlier, an ideal wound dressing is characterized by its ability to maintain a moist environment within the wound, provide protection against secondary infections, promote tissue regeneration, and enhance the overall quality of wound healing. Taking above factors into consideration, hydrogels have great potential as wound dressings [13], but on the other hand, there are many disadvantages that make nanofibers superior to them such as poor mechanical strength, poor mechanical stability, and bacterial permeability [14, 15].

1.2 Electrospinning

Electrospinning is the most widely used method for nanofiber production [16]. Electrospinning is a method that uses electric force to draw charged threads of polymer solutions or melted polymer to produce nanofibers [17]. An electro spinnable polymer melt or solution must be able to carry an electric charge and must have enough viscosity to be stretched without breaking up into droplets [18]. Three components are required for the electrospinning process to be completed: a voltage supplier, a capillary tube with a small-diameter needle (often a syringe), and a grounded collecting screen/drum. When the voltage (range of 1-30 kV) is applied, the hanging drop of polymer solution becomes highly electrified with an electric charge induced on the liquid surface. It is causes deformation of liquid drops into a conical object which named Taylor Cone [19].

Electrospun nanofiber membranes are a novel type of materials with various applications, including their use as wound dressings. These membranes possess a high surface-to-volume ratio, versatility, and significant microporosity. Electrospun nanofiber wound dressings, produced through electrospinning technology, offer numerous advantages. Firstly, their structure and biological functionality closely resemble the natural extracellular matrix (ECM), creating an optimal microenvironment for cell adhesion, proliferation, migration, and differentiation. Secondly, the polymer matrix used in electrospinning allows for the combination of the biocompatibility of natural polymers and the reliable mechanical strength of synthetic polymers [20].

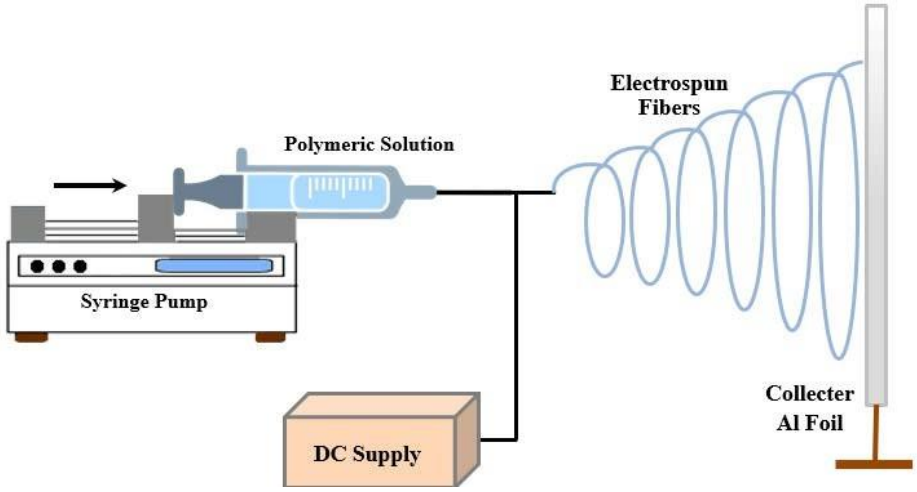

Figure 3: Schematic view of electrospinning process [21].

1.3 Nanoparticles

In this project, Polycaprolactone (PCL), Boric Acid (BA) and Zinc Oxide (ZnO) were used as nanofiber mat material. Many studies show that boric acid is a weak acid. It also has hydrophobic and highly moisture resistant properties. It is widely used as an antiseptic [22, 23]. Studies have demonstrated that it is also a successful agent in combating bacteria [24]. Its dilute solution is used as an eyewash and ear wash solution [25].

Polycaprolactone (PCL) is a preferred hydrophobic polymer to produce electrospun nanofibers due to its mechanical properties, good biocompatibility (no harm to nature), and ease of manufacture [26]. Meanwhile, PCL is a synthetic polymer with an extremely slow degradation rate that can regulate the rate of drug release from scaffolds [27].

Zinc oxide, a predominantly inert and white compound which is antibacterial, affordable, and nontoxic, finds extensive utilization as a bulking agent, filler, and white

pigment in numerous applications [28, 29]. When considering wound care, the primary focus revolves around expediting the skin's reparative processes. In this regard, zinc oxide plays a significant role, serving as a foundational component for protein synthesis and the development of enzymes. Upon contact with the skin, zinc oxide exerts exclusively beneficial effects [30].

1.4 Chitosan

Chitosan (CS) is a linear amino polysaccharide that is produced by deacetylation of chitin. Shellfish such as shrimp, lobster, and crab contain substantial amounts of the natural biopolymer chitin and therefore they are the main source of chitin [31]. The source, separation, and level of deacetylation of the chitin determine the quality of the chitosan [32].

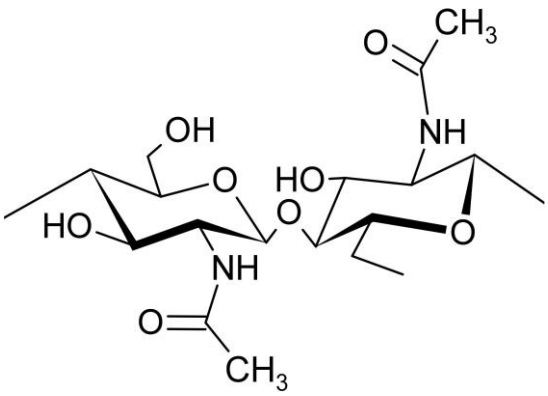

Figure 4: Chemical structure of chitosan [31].

Chitosan has many different biomedical uses. It can be used to help transfer drugs through the skin and as an antibacterial agent in medicine. It is also beneficial in bandages to stop bleeding. [31,33]. Chitosan is almost insoluble in water [34] and it is suitable for biomedical usage due to its low cost, high availability, low toxicity, biocompatibility, and anti-microbial activity [35]. Unlike chitin, chitosan is soluble in weak acids (pH < 6.3) like acetic acid [36,37]. Chitosan also speeds up the healing of wounds by activating fibroblasts, macrophages, and inflammatory cells. [38].

1.5 Hydrogels

Today, the biomedical use of hydrogels is quite common. Hydrogel refers to a mesh-like structure of interconnected polymers that can soak up and retain significant quantities of water, commonly employed in diverse fields like healthcare equipment, drug release mechanisms, and the cultivation of tissues [39]. Notably, owing to their hydrophilic nature, hydrogels can either provide moisture to the surrounding environment or maintain the moisture within the environment where they are utilized [40]. The extensive utilization of

hydrogels as wound dressings can be attributed to their unique blend of characteristics, including a high-water content, soft and flexible nature, and compatibility with biological systems [41]. Also, they can keep the wound warm and close [42]. The composition of hydrogel dressings can be tailored according to the specific characteristics of wounds, such as their size, severity, and location [40]. All the features mentioned above are the reasons why hydrogels are preferred in biomedical applications, especially wound dressings.

However, it should be noted that the strength of hydrogels is very low which means they are weak and act like brittle [43]. A variety of crosslinking techniques, including physical crosslinking, chemical crosslinking, and enzymatic crosslinking, can be used to make hydrogels stronger. In chemical crosslinking, it is recommended to crosslink hydrogels with chemicals such as formaldehyde or glutaraldehyde [44].

1.6 Chitosan-based Hydrogels

Chitosan is regarded as a highly suitable material for hydrogels because of its desirable properties such as biodegradability, biocompatibility, non-toxicity, antimicrobial activity, biological adhesion, biological activity, and hemostatic effects [45]. For this reason, chitosan was used in gel production in this project.

Figure 5 demonstrates the example mechanisms of chitosan-based hydrogels to promote wound healing [45].

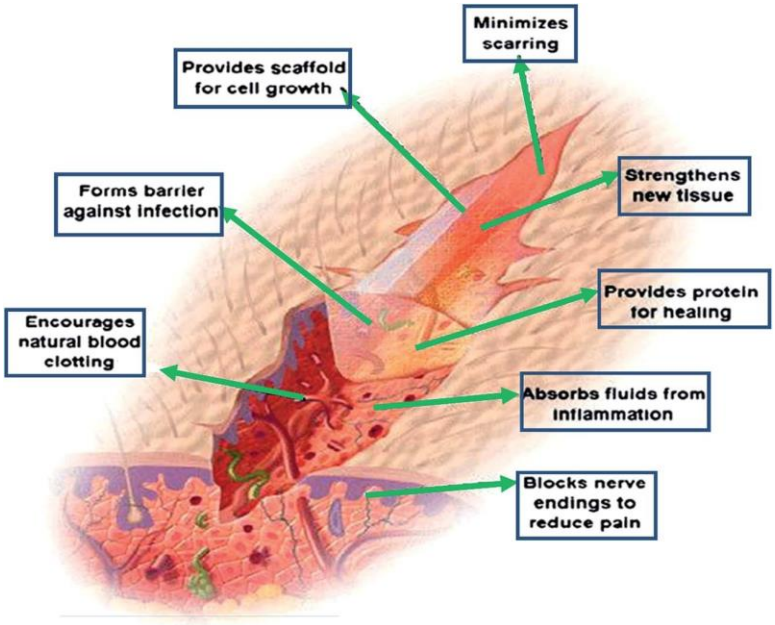

Figure 5: The mechanisms of chitosan-based hydrogels to promote wound healing [45].

This work demonstrates the mechanical characterization of chitosan based wound dressing materials reinforced with nanoparticles (PCL/ZnO/BA). Several tests were performed to demonstrate this characterization. These tests are tensile and compression test, contact angle test and swelling ratio tests.

1.7 Tensile Test

Tensile testing, also called tension testing, is a crucial examination in materials science and engineering that involves applying controlled tension to a specimen until it fractures. Key characteristics obtained from this test include ultimate tensile stress, fracture strength, maximum elongation, and reduction in cross-sectional area [46, 47]. Additional properties that can be deduced from these measurements include Young's modulus, Poisson's ratio, yield strength, and the behavior of strain-hardening. The preparation of tensile test specimens varies based on the specific test requirements. Typically, specimens have a standardized cross section, such as round or square, with two grip sections (shoulders) and a narrower gauge section in between. The grip sections enable secure handling of the specimen, while the gauge section indicates elastic deformation and eventual failure as it is stretched under the applied load [48].

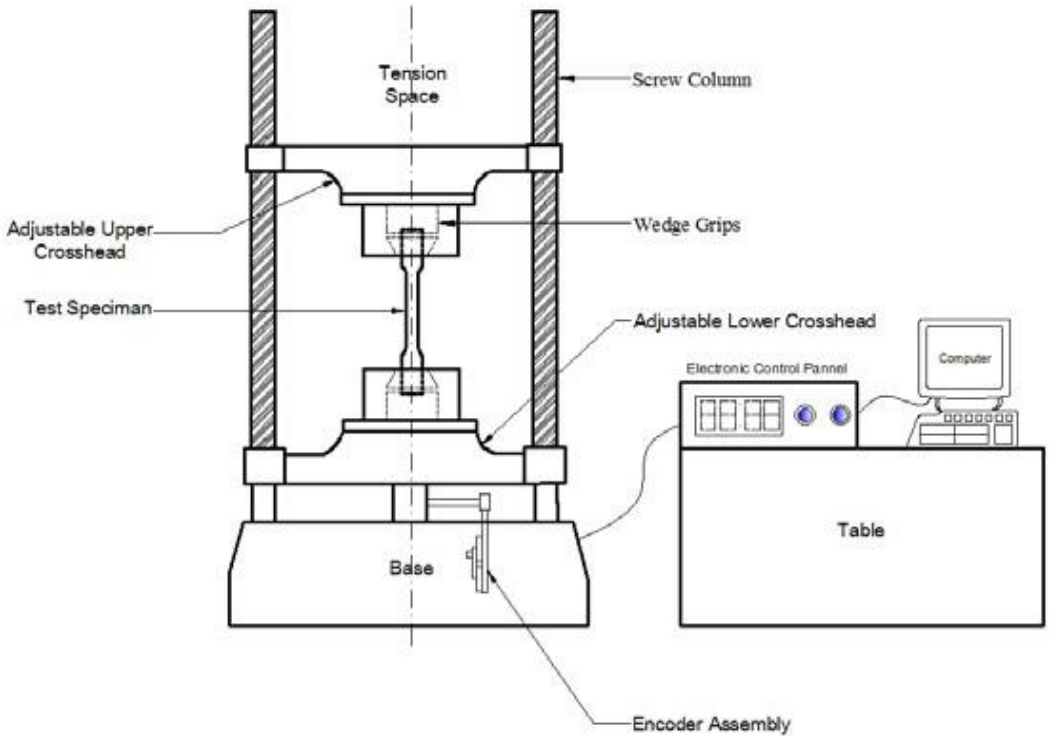

Figure 6: Schematic diagram of tensile testing machine [49].

After performing the tensile test, a graph should be drawn for the behavior and analysis of the material. This graph is the stress-strain graph. The strain, divided by the initial dimensions of the body, is the amount of deformation experienced by the body in the direction of the applied force [50]. Strain, a unitless quantity, can be calculated with the formula below:

$$\varepsilon = \frac{L - L_0}{L_0} \tag{1}$$

An example stress-strain plot is shown in Figure 7. A Linearity is first observed in the graph up to the proportionality point. Thanks to this linearity, a stress-strain relationship has been developed. This relationship is known as Hooke's Law:

$$\sigma = E * \varepsilon \tag{2}$$

where E is called Modulus of Elasticity or Young's Modulus. It is a material dependent quantity and unit of it is same as stress. Elastic modulus is defined as the ability of a material to resist elastic deformation when force is applied to it [51]. It can be easily found by finding the slope of the linear part of the stress-strain graph.

After proportionality limit point, graph starts to lose its linearity. Before that point graph shows a linear property. In the yield point, plastic deformations start. After this point, permanent shape changes begin even if the straining process is stopped. The deformation before the yield point is called elastic deformation and there are no permanent changes in the specimen. If the test is stopped, the sample returns to its original shape. The highest stress point reached in the stress strain diagram is called the ultimate strength point. Through this point, the maximum tensile stress can be found. After the highest stress is reached, a downward trend is seen on the graph and then the material fractures.

Not all stress-strain curves act like in Figure 7. The shape of the graph depends on material characteristics. For example, fracture occurs at low strains (before reaching plastic deformation zone) in brittle materials, while it takes some time and deformation for ductile materials to fracture (Figure 8).

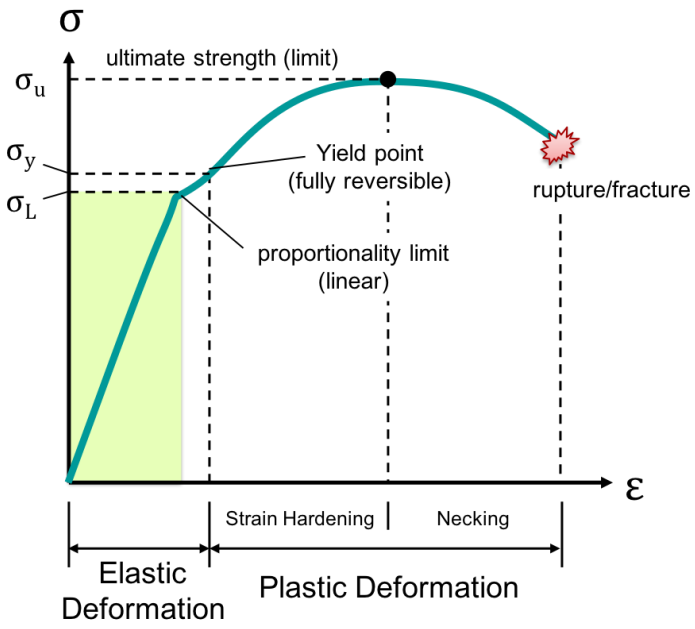

Figure 7 : Stress-strain curve [52].

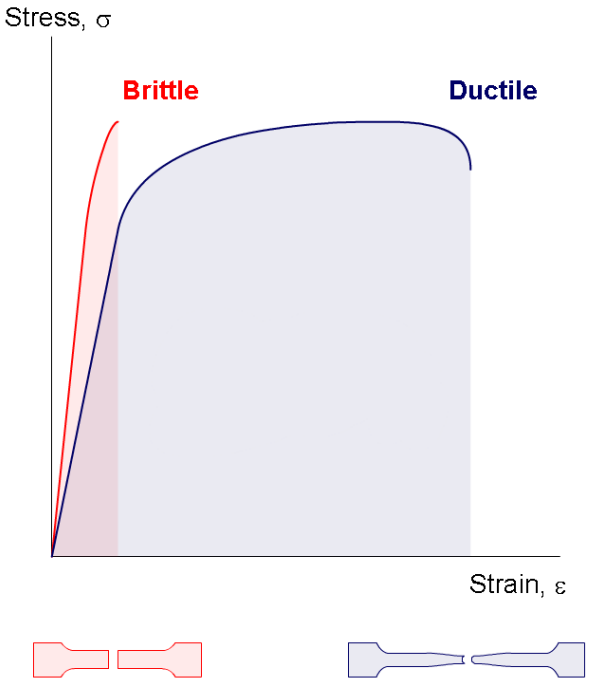

Figure 8: Different curve shapes for ductile and brittle materials [53].

In this project, tensile tests were made to compare the mechanical strengths and elongations of the fibers. These two properties are important in wound dressing materials due to their compatibility with external factors that may be encountered and physical movements.

1.8 Water Contact Angle Test (WCA)

The contact angle is the angle formed at the liquid-solid interface when observed through the liquid. It is employed to assess the degree of wetting or spreading of a liquid on a solid surface and can be calculated using the Young equation [54]. The measurement of water contact angle serves as a quantitative indicator of surface wettability and is a valuable technique for evaluating surface cleanliness. To determine the water contact angle, a drop is placed on the surface, and specialized software automatically analyzes the drop and records the corresponding contact angle value [55].

For contact angle, the sample is placed on the rotator. 1 drop is poured with a micro syringe pump. This moment is recorded with the camera. Then the reference line is drawn with the help of the computer and the contact angle is calculated automatically. Check Figure 9 for schematic diagram.

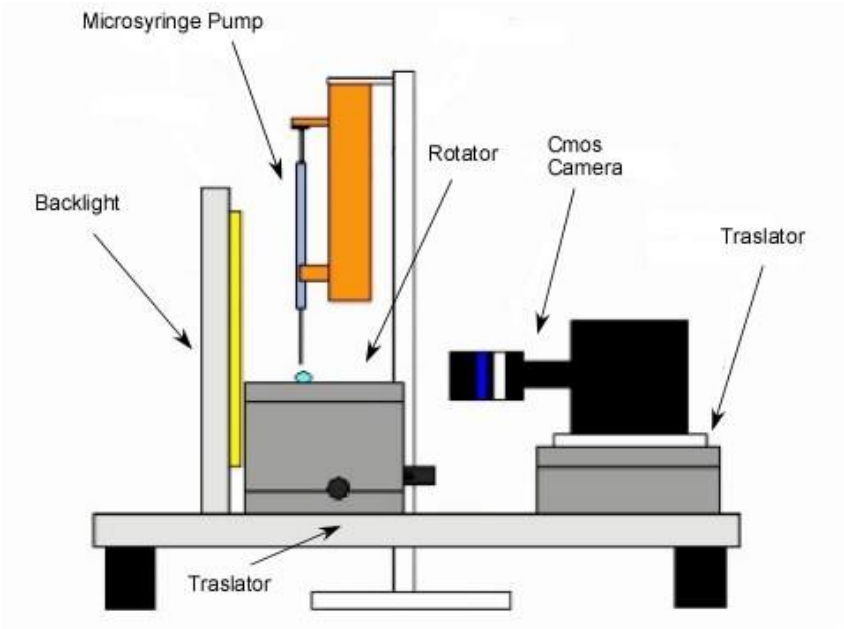

Figure 9: Schematic diagram of the contact angle goniometer [56].

The contact angle can vary between 0°, indicating complete wetting of a surface, and 180°, representing complete non-wetting. For water on a surface, a contact angle below 90° classifies the surface as hydrophilic, [57] while hydrophobic surfaces are defined by high-

water contact angles, typically equal to or greater than 90 degrees. Surfaces with water contact angles equal to or exceeding 150 degrees are referred to as superhydrophobic or ultra-hydrophobic. [58].

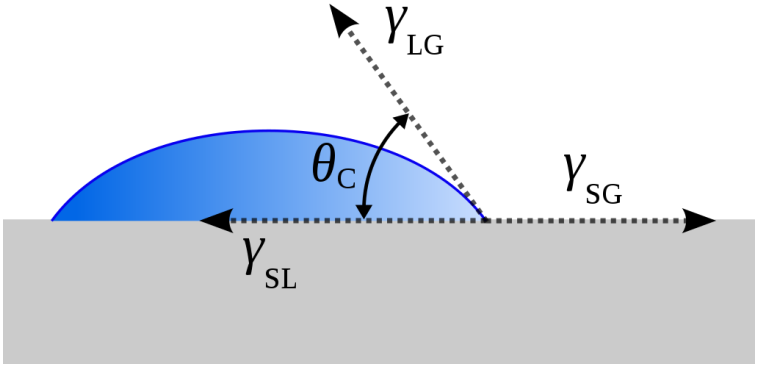

Figure 10: Schematic of a liquid drop [54].

The theoretical understanding of contact angle is based on the concept of thermodynamic equilibrium among three phases: the liquid phase (L), the solid phase (S), and the gas or vapor phase (G). If the solid–vapor interfacial energy is denoted by γ_{SG} the solid–liquid interfacial energy by γ_{SL} , and the liquid–vapor interfacial energy by γ_{LG} then the equilibrium contact angle θ_C is determined from these quantities by the Young Equation [54]:

$$\gamma_{SG} - \gamma_{SL} - \gamma_{LG} * cos\theta_C = 0 \quad (3)$$

Water contact angle tests were performed to determine the wettability and water absorption of the fibers and hydrogels. These properties are vital to adjust the moisture level of the wound.

1.9 Compression Test

The compression test is a method employed to evaluate the mechanical characteristics of various hydrogels [59]. It entails placing the hydrogel material between two plates and applying compression on to it (Figure 9) [60]. Thanks to this compression, the behavior of the material against crushing load is examined. It also enables measurement of the plastic deformation and limits of ductile fracture exhibited by the material. Compression testing plays a crucial role in quantifying the elastic and fracture properties of brittle materials or those with low ductility. It is employed to determine various essential parameters such as the modulus of elasticity, proportional limit, compressive yield point, compressive yield strength,

and compressive strength. These properties are vital for assessing the material's suitability for specific applications and its ability to withstand specific stress conditions without failure [61].

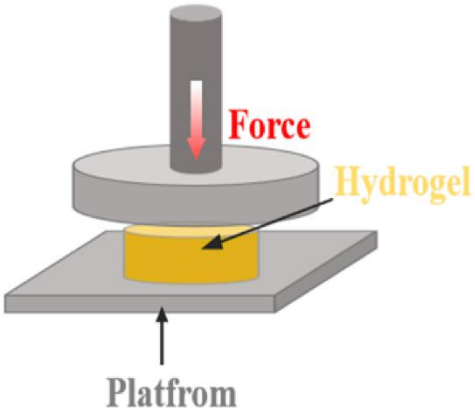

Figure 11: Schematic of a hydrogel compression testing [60].

1.10 Swelling Ratio

Swelling hydrogels in a solution liquid offers a simple, cost-effective, and safe approach to gathering valuable information about their characteristics. The data of swelling can be used to understand mechanical and viscoelastic properties, degradation rate, refractive index, and crosslinking degree [62]. The easiest way to obtain the swelling ratio is by measuring the weight of hydrogel before and after swelling. The volume swelling ratio can be calculated by utilizing the known densities of the polymer and solvent. By applying these density values, the change in volume of the hydrogel can be accurately determined [63].

Water-absorbing capability determines a membrane's swelling ratio. The swelling test consists of 4 parts. First, the mass of the dried sample is measured, then, the specimen is dropped in the desired liquid or solution (usually water), after some time passes the removed specimen gets weighed again with all the absorbed liquid. The dry weight gets extracted from the wet weight and the result gets divided by the dry weight. This process shows us how much water the dry state of the specimen can hold.

$$SR\ (\%) = \frac{W_s - W_D}{W_D} * 100 \qquad (4)$$

2) MATERIAL AND METHODS

2.1 NANOFIBROUS MATS

2.1.1 Materials

Chloroform ($CHCl_3$) with the density of 1.47 g/cm^3 and (CH_3CN) with the density of 0.786 g/cm^3 were obtained from ISOLAB. PCL with the density of 1.145 g/cm^3 was obtained from Aldrich. ZnO with the density of 5.61 g/cm^3 was purchased from Balmumcu Kimya. Boric Acid with the density of 1.435 g/cm^3 was purchased from Başak Kimya.

2.1.2 Preparation of Solutions for Electrospinning

First, 14.45 g of chloroform and 2.55 g of acetonitrile were mixed. Then 3g PCL was added to this mixture. This final mixture was called the control group. In other solutions, 2%, 4%, 6% and 10% of 3 grams were prepared as boric acid and the remainder was PCL (Figure 12). The same process was applied for ZnO solutions (Figure 13). The resulting mixtures were stirred at 200 rpm for 24 hours in a magnetic stirrer at 50°C. Then, they were rested at room temperature for 2-3 hours to remove air bubbles.

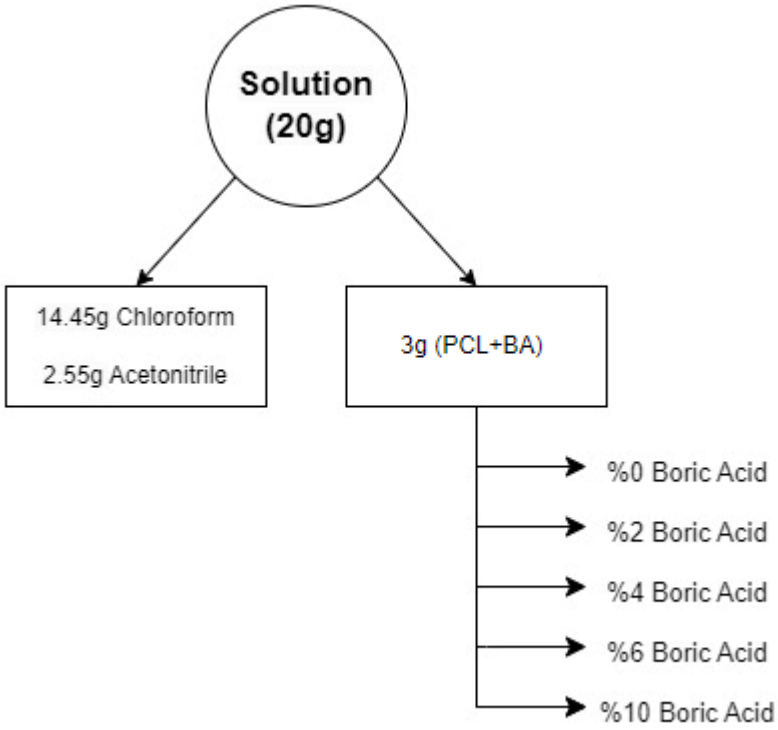

Figure 12: Material quantities of PCL and boric acid solutions.

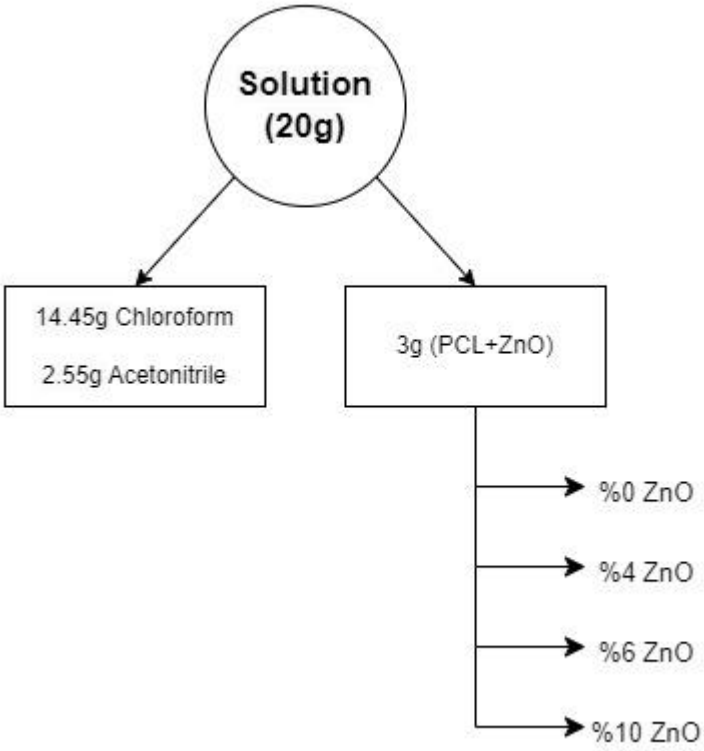

Figure 13: Material quantities of PCL and ZnO solutions.

Figure 14: Example of PCL and BA solution.

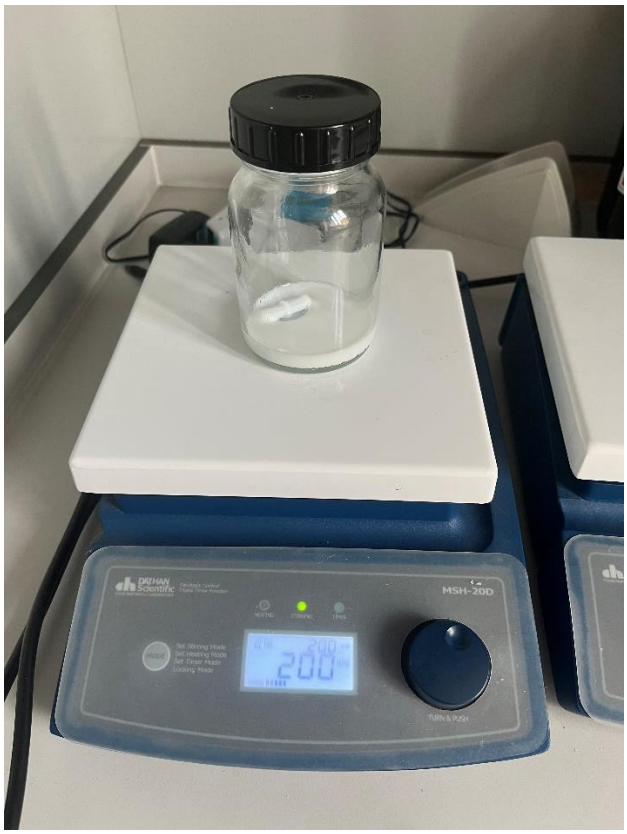

Figure 15: Example of PCL and ZnO solution.

The densities of the solutions were calculated with the mixture density formula (Table 1). It was observed that the densities increased as Boric Acid and Zn concentrations increased.

Table 1: Calculated densities of solutions.

Nanofibers	**Density (g/cm^3)**
PCL	1.274
PCL/BA%2	1.275
PCL/BA%4	1.277
PCL/BA%6	1.277
PCL/BA%10	1.279
PCL/ZnO%4	1.281
PCL/ZnO%6	1.285
PCL/ZnO%10	1.292

2.1.3 Nanofiber fabrication

10 mL of the solution, which was free of air bubbles, was taken with the help of a syringe. "Inovenso NE 200 Nanospinner" was used as an electrospinning machine. The syringe was attached to the pump and the flow rate of solution was 1 mL/h whereas the distance between the rotating drum collector and the nozzle was 25 cm. A 20 kV voltage was supplied (Figure 16). The temperature was kept constant at 25°C respectively throughout the fabrication process. In addition, greaseproof paper was wrapped around the collector drum for easier separation of the fibers from the drum.

At the tip of the nozzle, the nanofiber solution could dry and harden, so the nozzle could be clogged. For this reason, the nozzle was cleaned regularly. The same parameters and procedures were applied for all nanofiber mats.

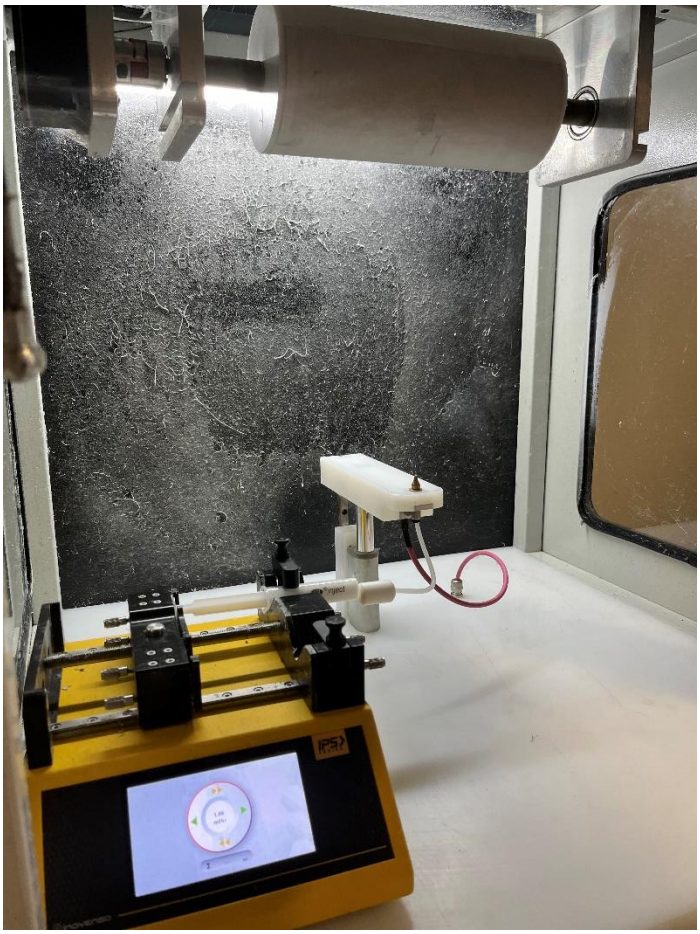

Figure 16: Electrospinning setup.

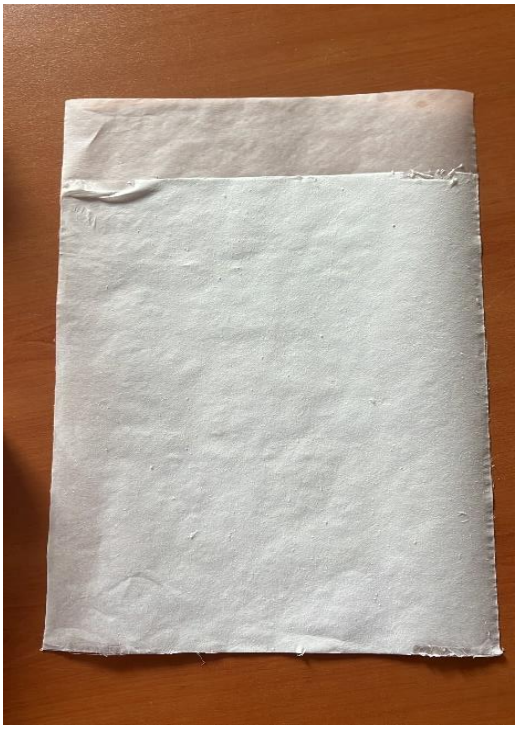

Figure 17: Electrospun nanofiber mat sample (%6 ZnO).

2.1.4 Tensile Test

For tensile testing, 60x10mm specimens were cut from electrospun mats. In addition, 60x45mm and 10mm thick paper frames were prepared. The cut fiber mat was attached to the frame with double-sided tape and water-based adhesive. In addition, cardboard was glued on both grip sides to increase the grip thickness (Figure 18). "Shimadzu AGS-X 50 kN" is used as tensile testing machine. The test specimen (test window frame with the fiber) was mounted on the tensile tester such that the grip is on the tabs holding the fiber membrane. The left and right edge of the window frame is cut as shown in Figure 19. The samples were stretched with a strain rate of 5 mm/min until breakage [64, 65, 66, 67]. The gauge length was 40 mm.

Also, "Instron 4411 Tensile Strength Tester" is used as the tensile tester, which is more suitable for fine fiber mats (Figure 20). All the rest of the sample preparation was the same, except for using cardboard to thicken the grips. In addition, different strain rates were tried to observe the effect of strain rate, and finally, 30mm/min, which was observed to be cleaner in graphics, was preferred. The gauge length was again 40 mm. Each sample was tested 3 times.

Figure 18: Test specimen sample (First case).

Figure 19: Tensile test setup (first case).

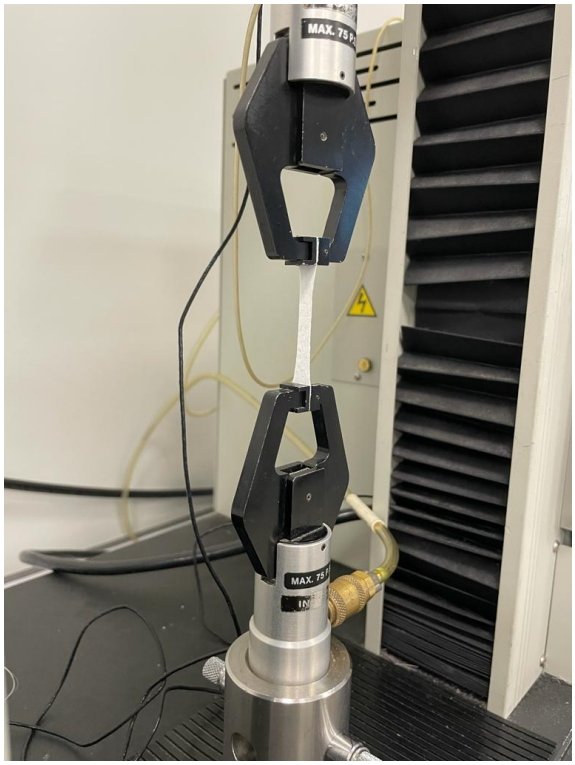

Figure 20: Tensile test setup (second case).

2.1.5 Water Contact Angle Test

The hydrophobicity and wettability of nanofiber mats was measured by water contact angle measurements. Each film was cut into 30x20 mm and placed on the test table. “KSV CAM 101 " was used as the contact angle measuring device. All samples were tested 3 times.

2.2 HYDROGELS

2.2.1 Materials

95% deacetylated Chitosan was purchased from BIYOPOL. 50% purity glutaraldehyde was purchased from Alfasol. Polyvinyl Alcohol (PVA) and acetic acid were purchased from Başak Kimya. Deionized distilled water was purchased from BRTR Kimya.

2.1.2 Preparation of Chitosan Hydrogels

4 g of chitosan was dissolved in 100 mL of 1.0% aqueous acetic acid at 75°C with continuous stirring to obtain a pale-yellow viscous chitosan solution. Then, 2 g of PVA is stirred in 100 mL of distilled water at 75°C until it is completely dissolved. Then, these mixtures were left to rest for 1-2 hours to get rid of air bubbles. After resting, they were cooled in the refrigerator. Cold CS and PVA solutions were mixed with each other in certain rates, then 2% Glutaraldehyde solution was added for crosslinking. The final mixture was poured into molds and left at room temperature for 24h to dry. The mentioned ratios are listed in Table 2.

Table 2: Content ratios and names of hydrogels.

Hydrogel Names	**Solution Amounts (mL)**		
	%4 CS	%2 PVA	%2 GA
CS12	12	0	2
CS8	8	4	2
CS6	6	6	2
CS4	4	8	2

2.1.3 Compression Test

"Shimadzu AGS-X 50 kN" is used as compression testing machine. Strain rate was preferred as 5mm/min [68]. 12mm height and 30mm diameter cylindrical shaped hydrogels were used as specimen. Each gel was tested 3 times at room temperature.

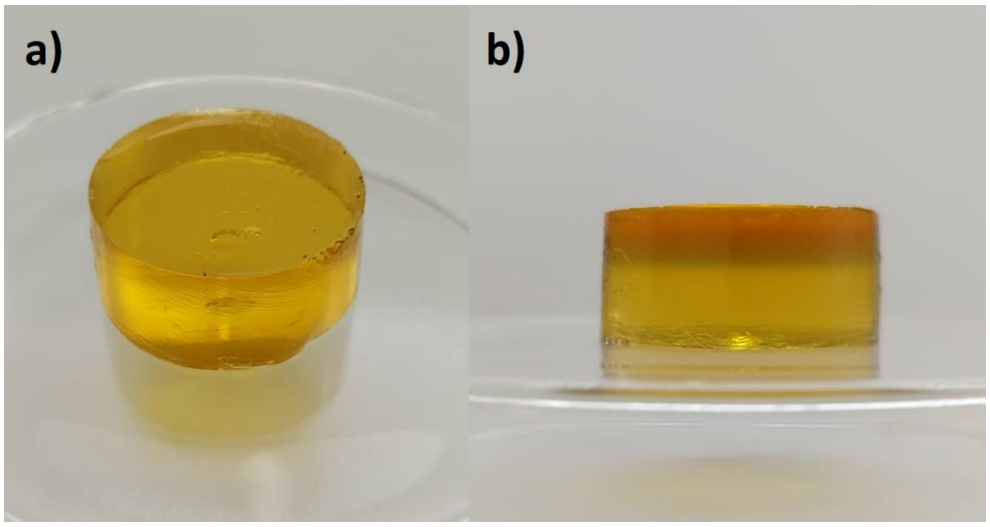

Figure 21: Hydrogel test specimens, **a)** Isometric view, **b)** Front view.

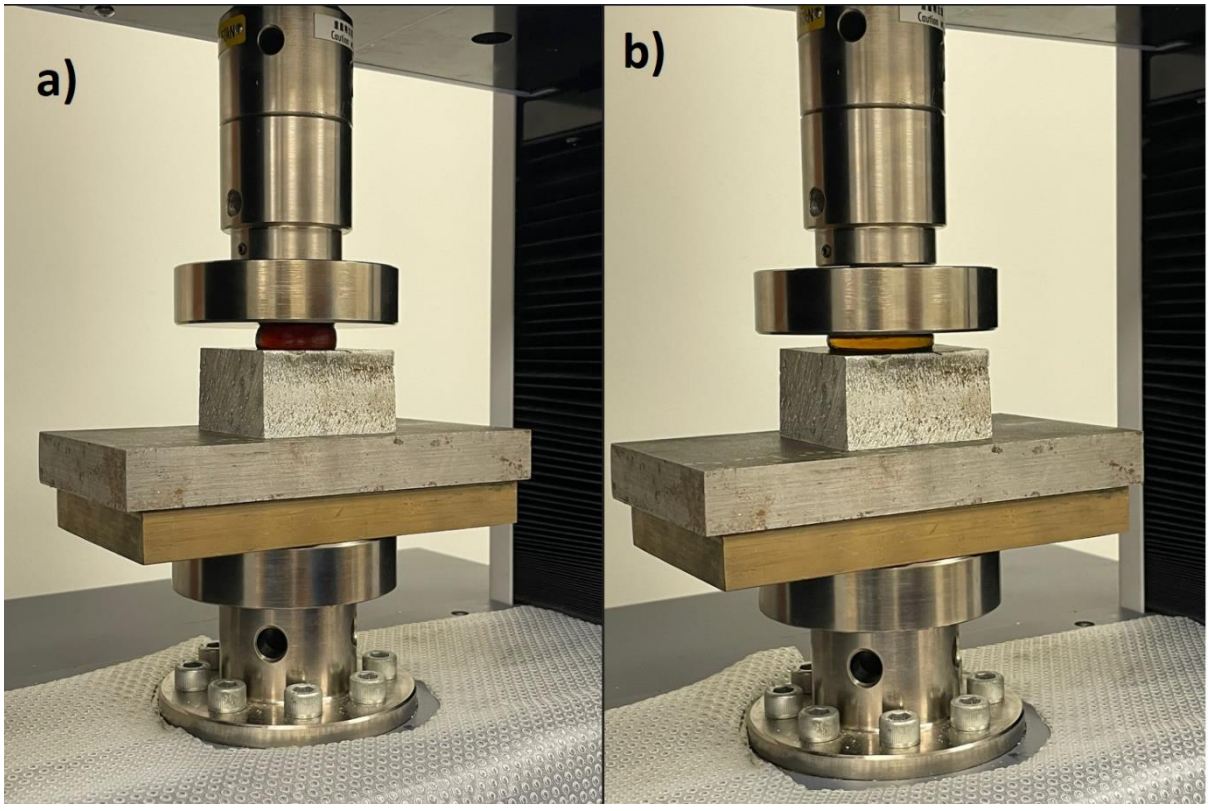

Figure 22: Hydrogels in compression test.

2.1.4 Water Contact Angle Test

The hydrophobicity and wettability of hydrogels were measured by water contact angle measurements. Each film was cut into rectangular shape to obtain a flat surface and placed on the test table. “KSV CAM 101 " was used as the contact angle measuring device. All samples were tested 3 times.

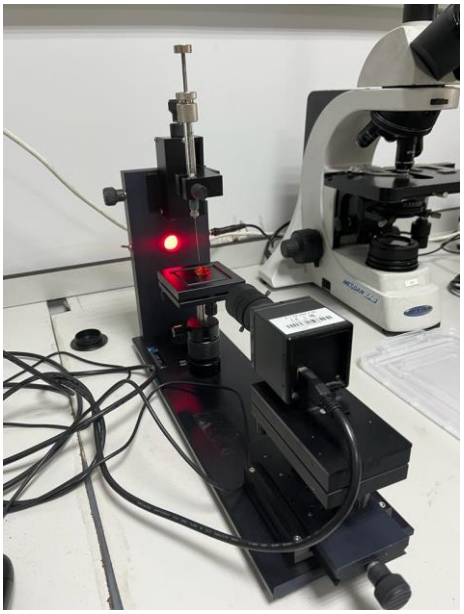

Figure 23: Contact angle test setup.

2.1.5 Swelling Ratio Test

The gels were incubated in 1% saline for a total of 24 hours. Weights were checked at 4th, 8th and 24th hours. Salt water was used to imitate a structure like sweat. As it is known, this dressing material will be adhered to the skin, and therefore the liquid that will come into contact with the most is sweat.

Figure 24: Experiment setup for swelling ratio.

3) CALCULATIONS AND RESULTS

3.1 NANOFIBROUS MATS

3.1.1 Tensile Test

The thicknesses of the specimens were measured with "Mitutoyo ABS Digital Thickness Gauge". All samples were measured from 3 different points. The results are listed in Table 3.

Table 3: Thickness of nanofiber mats

Nanofibers	Thickness (mm)			
	1st Specimen	2nd Specimen	3rd Specimen	Mean
PCL	0.257 ±0.010	0.218 ±0.005	0.205 ±0.002	0.227 ±0.013
PCL/BA%2	0.208 ±0.003	0.231 ±0.002	0.202 ±0.001	0.214 ±0.007
PCL/BA%4	0.182 ±0.005	0.173 ±0.001	0.176 ±0.003	0.177 ±0.003
PCL/BA%6	0.224 ±0.009	0.163 ±0.002	0.193 ±0.004	0.193 ±0.014
PCL/BA%10	0.236 ±0.007	0.228 ±0.002	0.250 ±0.005	0.238 ±0.006
PCL/ZnO%4	0.297 ±0.007	0.288 ±0.004	0.278 ±0.001	0.288 ±0.005
PCL/ZnO%6	0.179 ±0.001	0.184 ±0.003	0.169 ±0.001	0.177 ±0.004
PCL/ZnO%10	0.162 ± 0.004	0.161 ± 0.006	0.152 ±0.002	0.157 ±0.004

Tensile stress and Elastic Modulus can be calculated with the formulas below:

$$\sigma_t = \frac{F_t}{A} \tag{5}$$

$$E = \frac{\sigma}{\varepsilon} \tag{6}$$

Maximum tensile loads are listed in Table 4 for both strain rates are 5mm/min and 30mm/min. Table 5 and 6 demonstrates tensile stress and strain at break values of fibers for $\dot{\varepsilon}$=5mm/min and $\dot{\varepsilon}$=30mm/min, respectively.

In the test where the strain rate was 5mm/min, too much fluctuation was seen in the graphics. Because of these fluctuations, curve fitting methods were applied to the data to obtain smoother graphs and better comparisons.

Table 4: Maximum loads that fibers experienced

Nanofibers	Force (N)	
	$\dot{\varepsilon}$ = 5mm/min	**$\dot{\varepsilon}$ = 30mm/min**
PCL	2.329	2.509 ±0.141
PCL/BA%2	1.828	1.949 ±0.055
PCL/BA%4	1.756	1.415 ±0.040
PCL/BA%6	1.931	1.898 ±0.150
PCL/BA%10	1.979	1.936 ±0.113
PCL/ZnO%4	2.480	2.817 ±0.047
PCL/ZnO%6	2.233	1.808 ±0.078
PCL/ZnO%10	1.852	1.813 ±0.024

Table 5: Tensile stress and strain at break values of fibers ($\dot{\varepsilon}$=5mm/min)

Nanofibers	Ultimate Tensile Stress (MPa)	Strain at Break (%)
PCL	1.027	88.25
PCL/BA%2	0.855	173.90
PCL/BA%4	0.992	146.86
PCL/BA%6	0.999	182.53
PCL/BA%10	0.831	143.05
PCL/ZnO%4	0.862	113.58
PCL/ZnO%6	1.260	84.88
PCL/ZnO%10	1.169	69.59

Table 6: Tensile stress and strain at break values of fibers (ε̇=30mm/min)

Nanofibers	Ultimate Tensile Stress (MPa)	Strain At Break (%)	Elastic Modulus (MPa)
PCL	1.108 ±0.049	148.4 ±8.8	7.000 ±0.758
PCL/BA%2	0.917 ±0.089	262.7 ±15.3	4.249 ±0.555
PCL/BA%4	0.801 ±0.052	197.7 ±14.3	4.445 ±0.141
PCL/BA%6	0.984 ±0.076	263.5 ±5.4	4.789 ±0.402
PCL/BA%10	0.811 ±0.050	162.5 ±12.4	4.817 ±0.390
PCL/ZnO%4	0.980 ±0.010	164.5 ±4.3	6.097 ±0.082
PCL/ZnO%6	1.021 ±0.069	107.3±8.5	8.261 ±1.218
PCL/ZnO%10	1.145 ±0.031	122.6 ±7.5	9.034 ±0.563

Figures 25, 26 and 27 demonstrate the stress-strain curves when strain rate is 30mm/min and Figure 28 demonstrate the stress-strain curve when strain rate is 5mm/min.

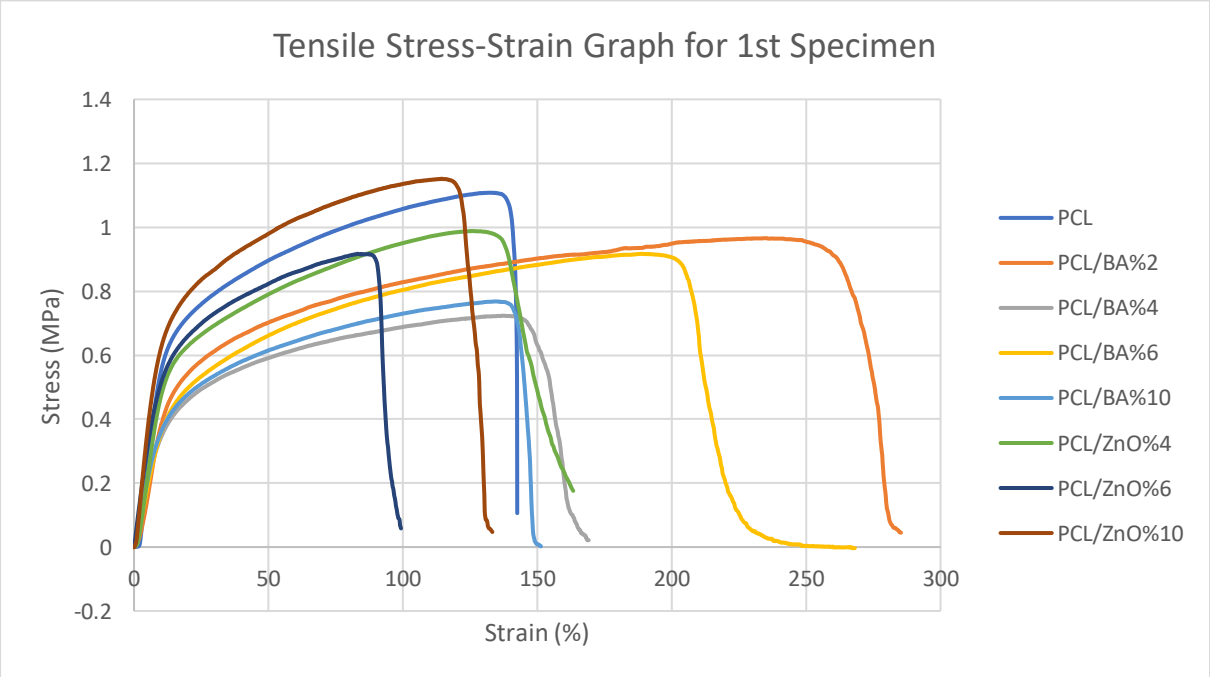

Figure 25: Stress strain graphs for 1st specimen (ε̇=30mm/min).

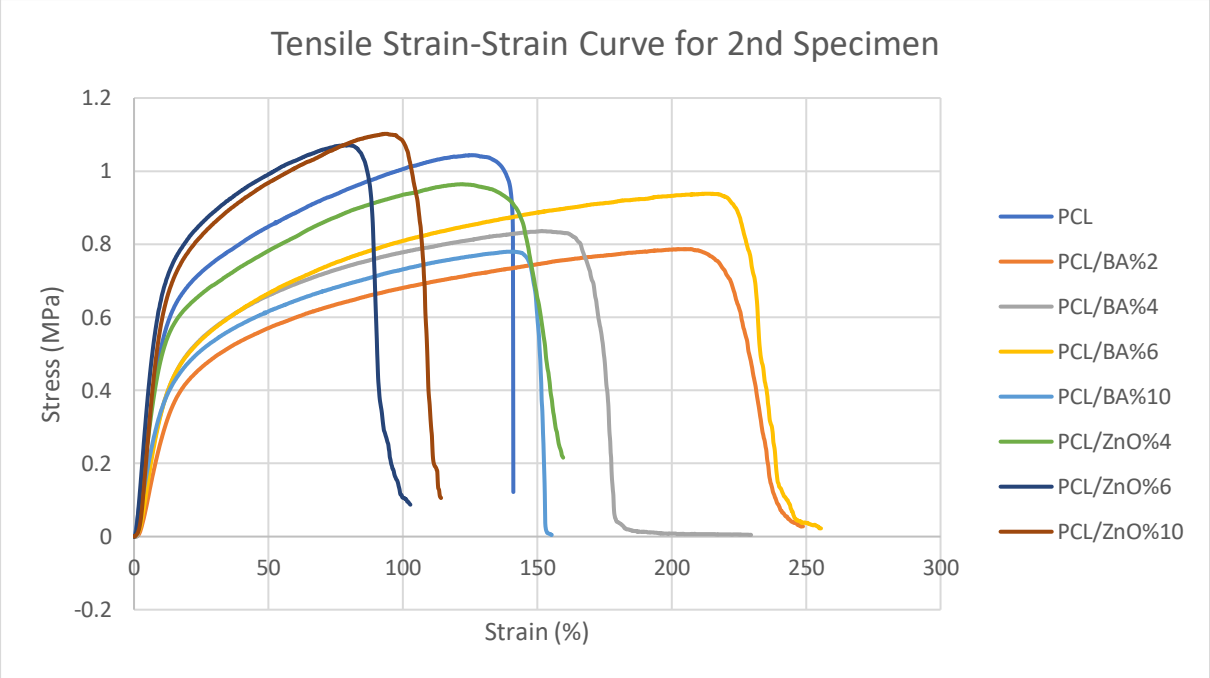

Figure 26: Stress strain graphs for 2nd specimen (ε̇=30mm/min).

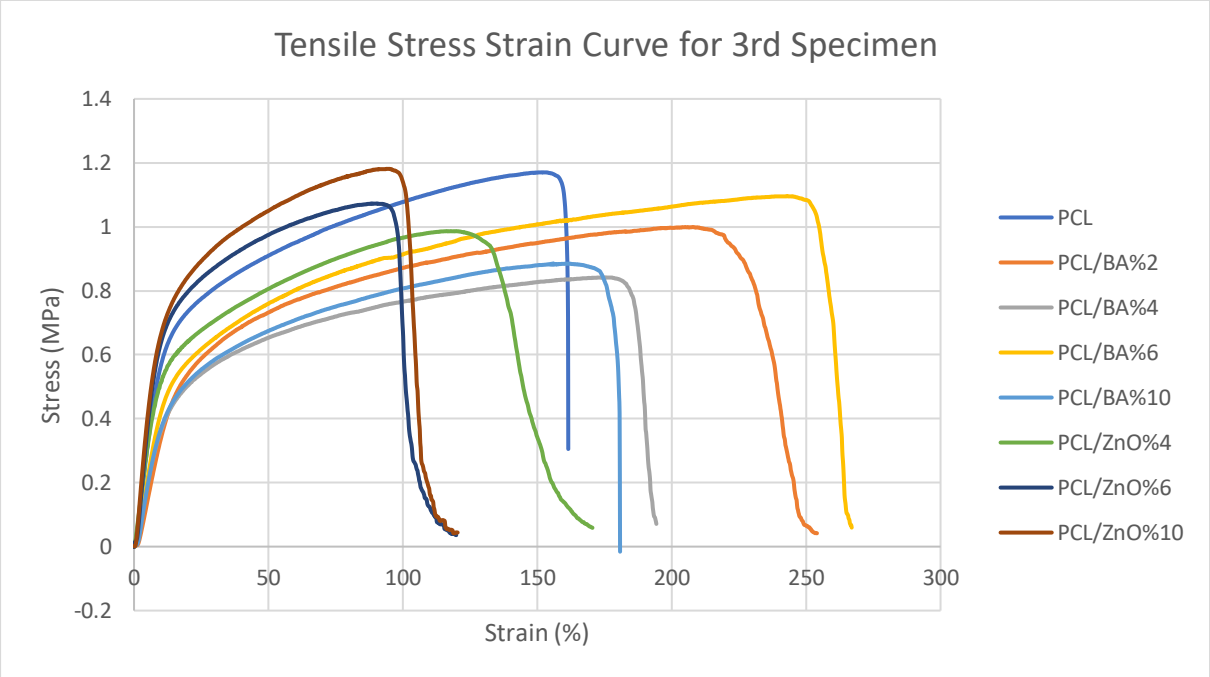

Figure 27: Stress strain graphs For 3rd specimen (ε̇=30mm/min).

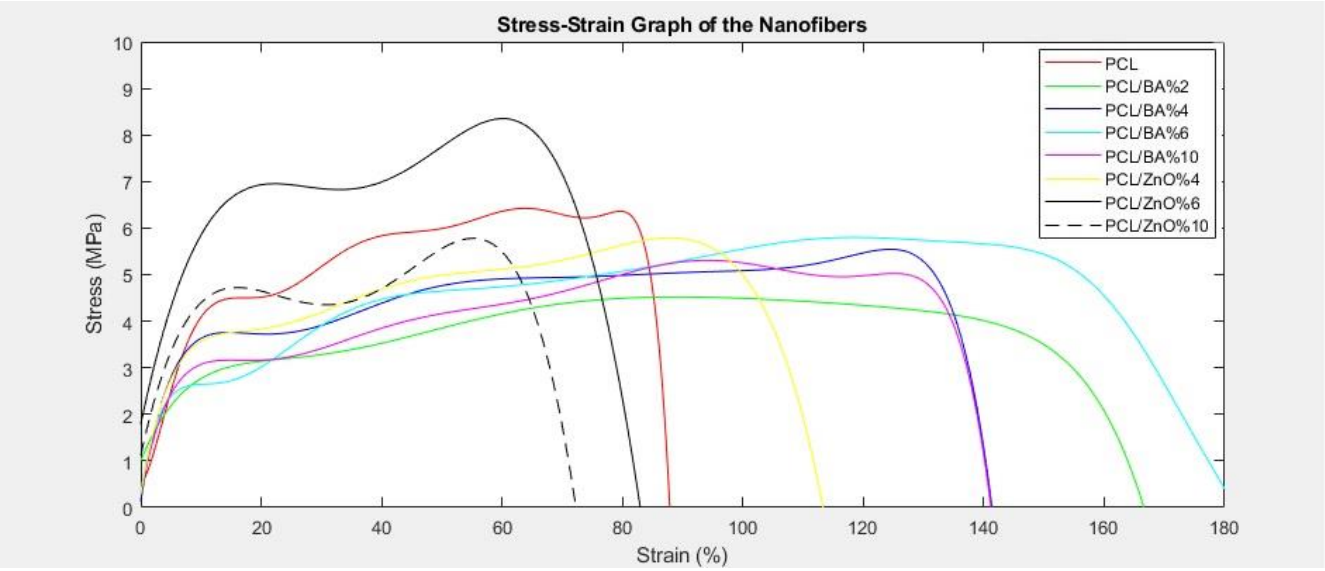

Figure 28: Stress strain graphs (ε̇=5mm/min).

3.1.2 Water Contact Angle Test

The results of the water contact angle tests for fiber specimens are listed in Table 7 and 8. Results are also plotted in Figure 29 for better comparison.

Table 7: Contact angle measurements of PCL/BA specimens.

Nanofiber	Contact Angle (°)
PCL	123.67 ± 2.50°
PCL/BA%2	119.81 ± 4.30°
PCL/BA%4	121.34 ± 3.65°
PCL/BA%6	115.11 ± 1.32°
PCL/BA%10	113.79 ± 2.70°

Table 8: Contact angle measurements of PCL/ZnO specimens.

Nanofiber	Contact Angle (°)
PCL	123.67 ± 2.50°
PCL/ZnO%4	114.74 ± 1.56°
PCL/ZnO%6	113.79 ± 1.97°
PCL/ZnO%10	115.48 ± 1.11°

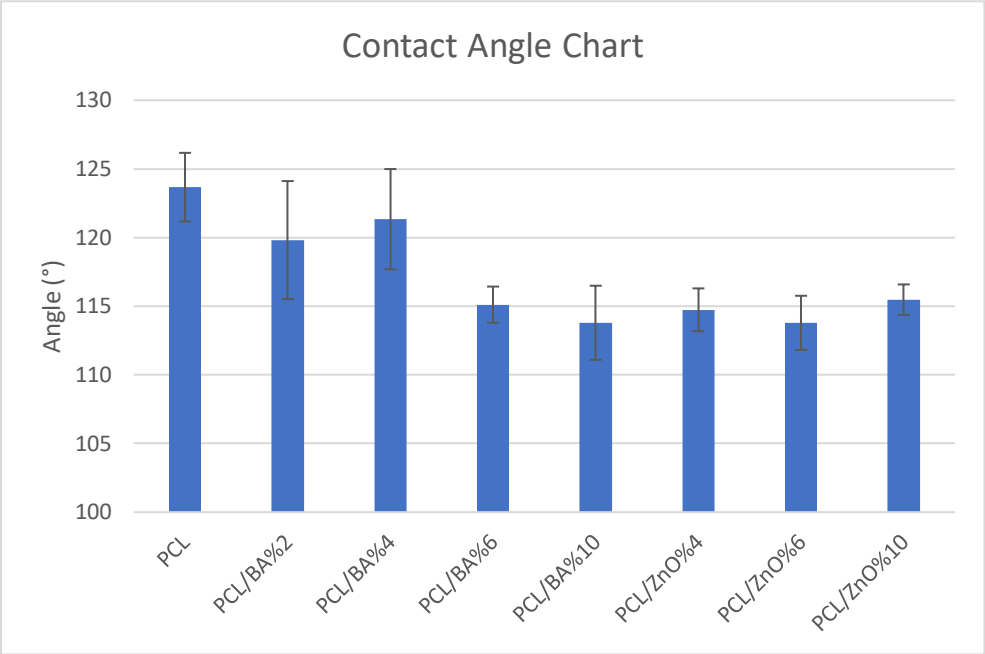

Figure 29: Contact angle chart for fibers

Figure 30 is images taken by computer when the water drop touches the nanofiber mat surfaces.

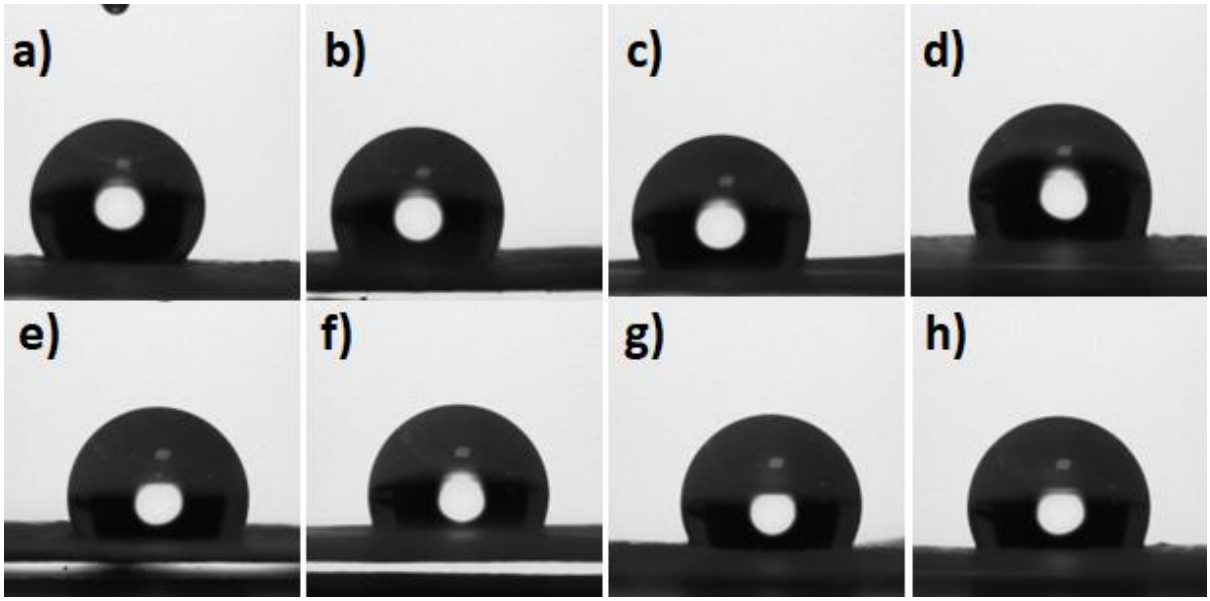

Figure 30: Contact angle images of **a)** PCL, **b)** PCL/BA%2, **c)** PCL/BA%4, **d)** PCL/BA%6, **e)** PCL/BA%10, **f)** PCL/ZnO%4, **g)** PCL/ZnO%6, **h)** PCL/ZnO%10.

3.2 HYDROGELS

3.2.1 Water Contact Angle Test

The contact angle test was measured both when the drop touched the gel and after 30 seconds. The data are listed in Table also results are plotted in Figure 31 for better comparison.

Table 9: Contact angle results of hydrogels.

Gels	Contact Angle (°) first contact	Contact angle (°) after 30s
CS12	82.84 ±4.24	70.51 ±4.83
CS8	93.78 ±0.65	71.50±3.99
CS6	87.38 ±2.41	66.50 ±2.65
CS4	72.76 ±2.62	53.32 ±5.22

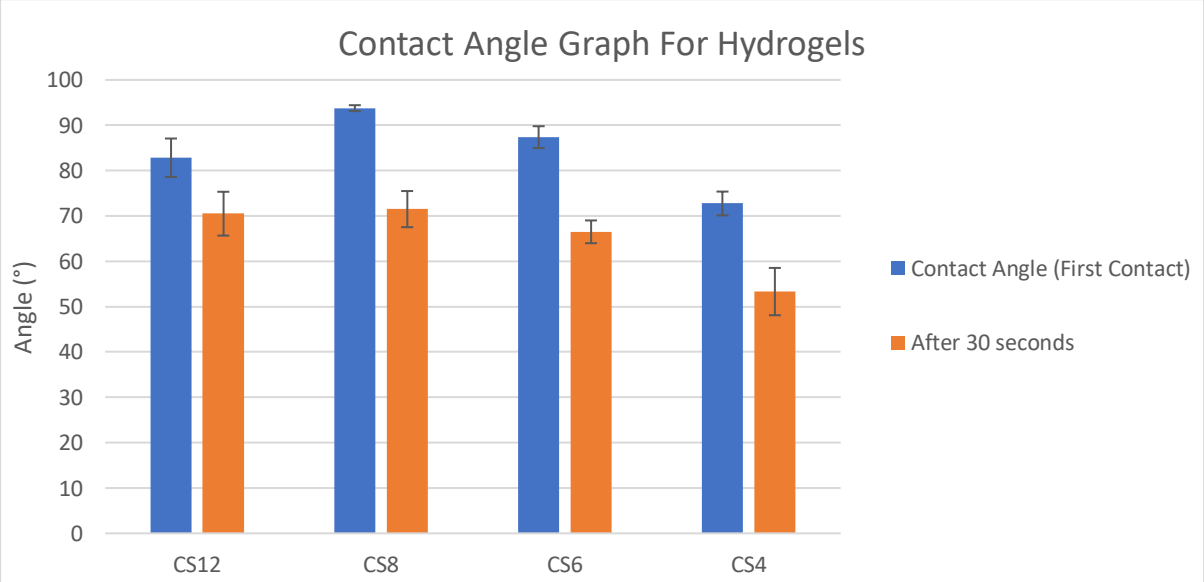

Figure 31: Contact angle graph for hydrogels.

Figures 32-35 are images taken by computer when the water drop touches the nanofiber mat surfaces. Among these, figures marked with (a) represent the first contact, and figures marked with (b) represent the contact after 30s.

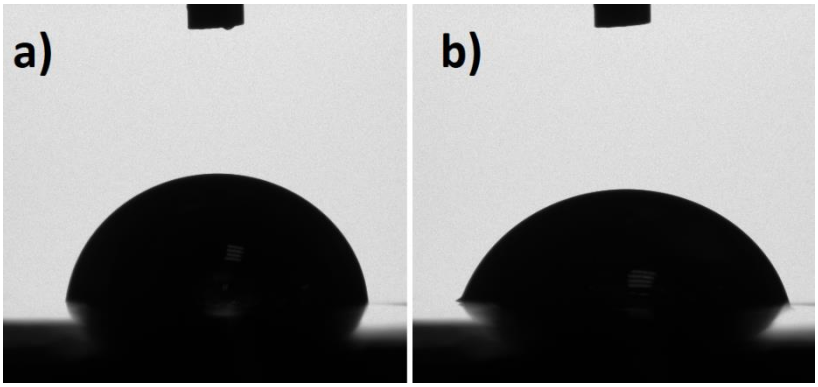

Figure 32: Contact angle of CS12, **a)** first contact, **b)** after 30s.

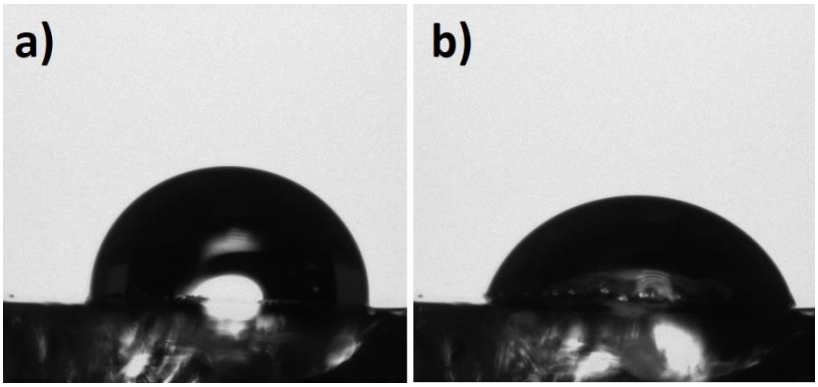

Figure 33: Contact angle of CS8, **a)** first contact, **b)** after 30s.

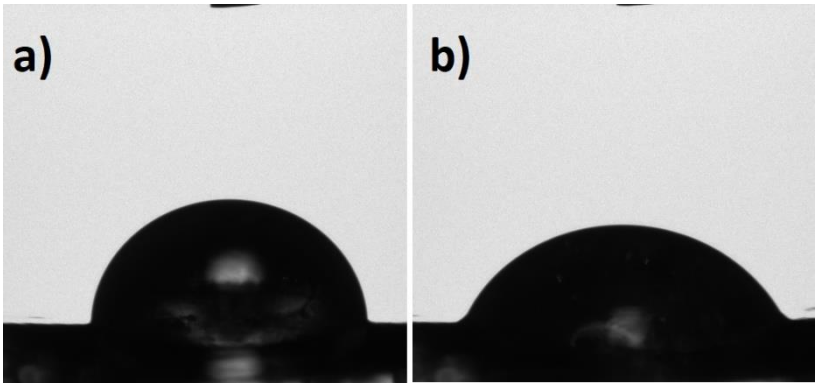

Figure 34: Contact angle of CS6, **a)** first contact, **b)** after 30s.

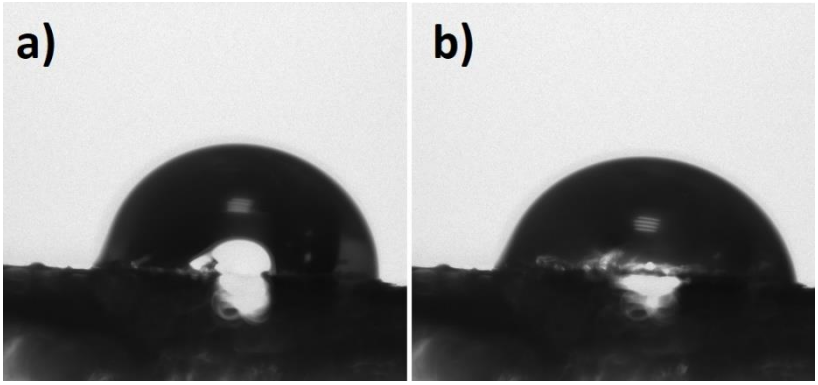

Figure 35: Contact angle of CS4, **a)** first contact, **b)** after 30s.

3.2.2 Compression Test

The results of the compression test were listed in Table 10. Ultimate compression stress was calculated with the formula below:

$$\sigma_c = \frac{F_c}{A} \tag{7}$$

Table 10: Results of compression test.

Gels	Ultimate Compression Stress (MPa)	Compressive Strain at Break (%)
CS12	0.118 ±0.016	56.57 ±3.17
CS8	0.094 ±0.018	67.46 ±3.74
CS6	0.073 ±0.018	68.77 ±4.81
CS4	0.050 ±0.008	73.86 ±3.62

Figures 36, 37 and 38 demonstrate the compressive stress-strain curves for hydrogel specimens.

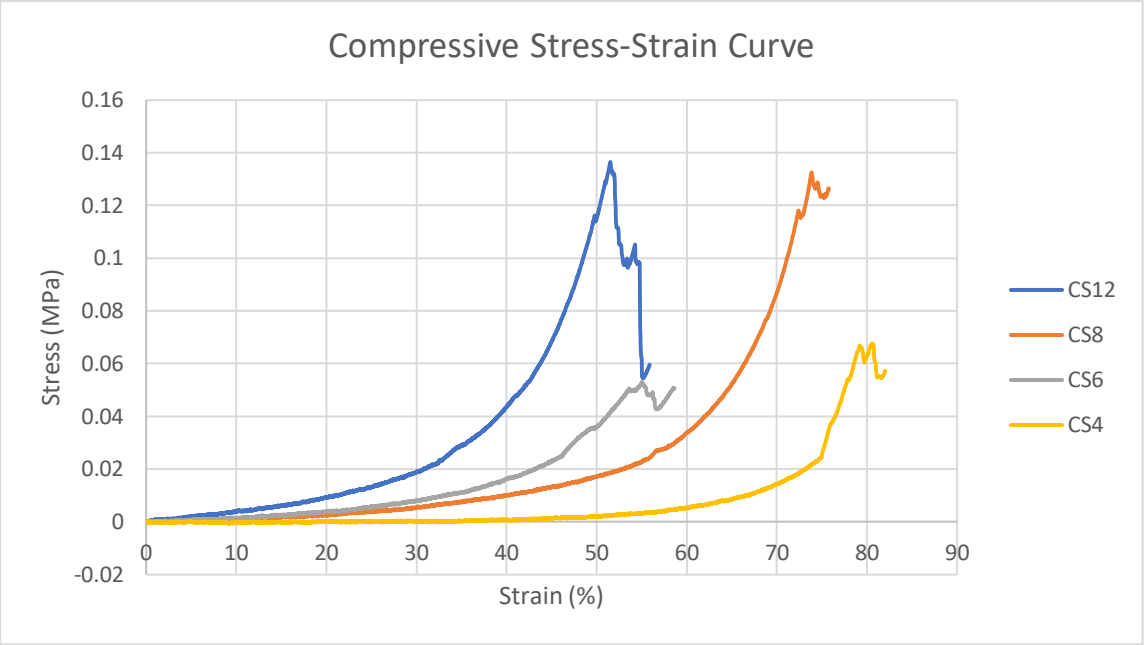

Figure 36: Compressive stress-strain graph for 1st specimen.

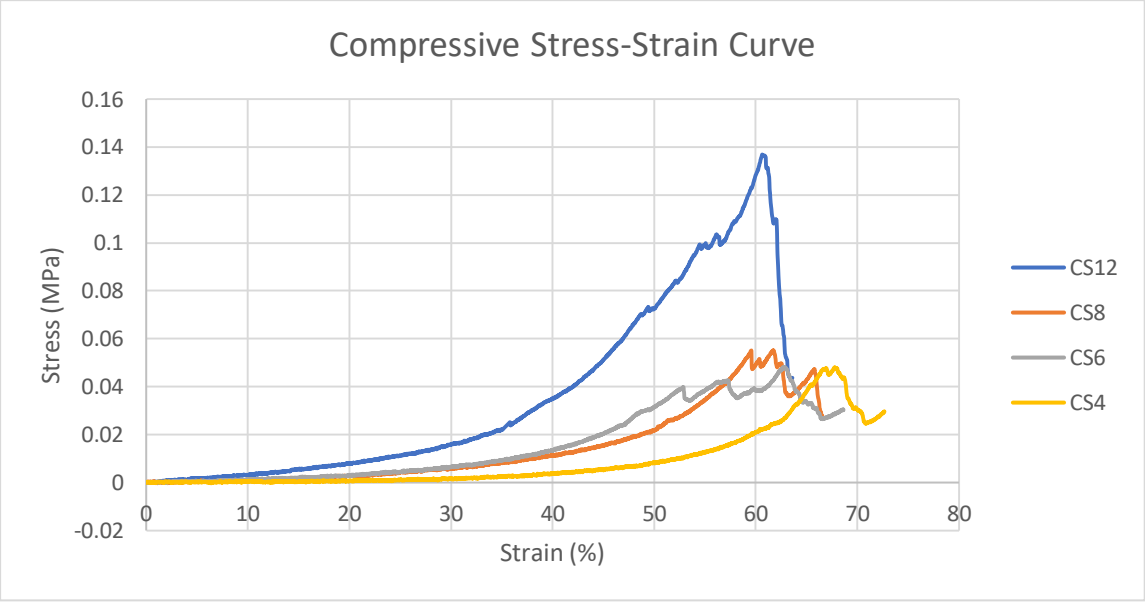

Figure 37: Compressive stress-strain graph for 2nd specimen.

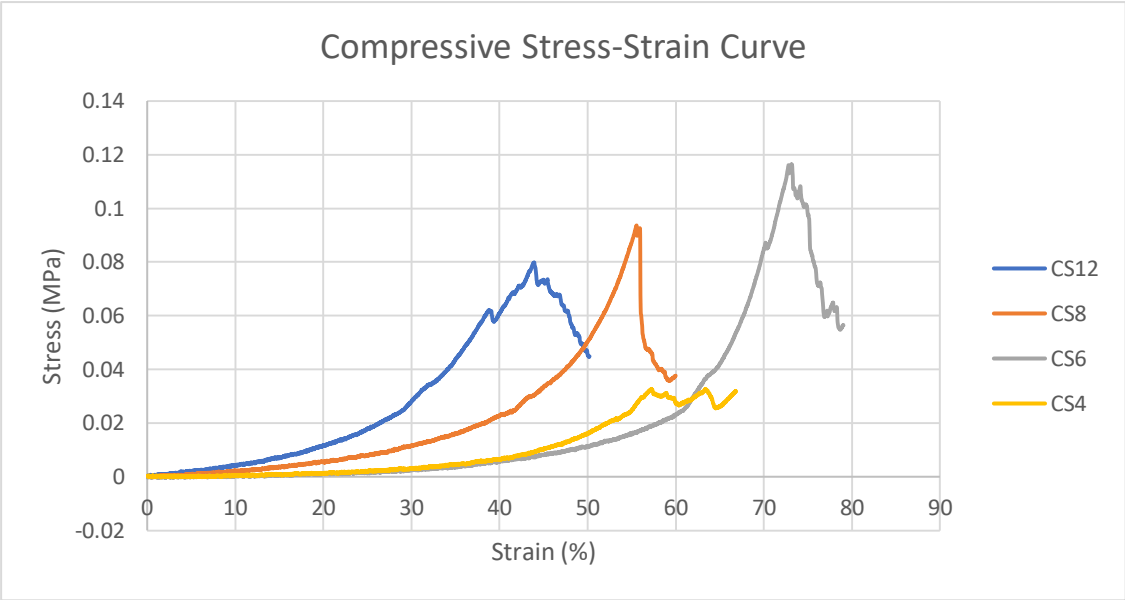

Figure 38: Compressive stress-strain graph for 3rd specimen.

3.2.3 Swelling Ratio Test

Swelling ratio calculations were made using the equation 4 and results were written in Table 11. Also, results were plotted in Figure 39 for better comparison.

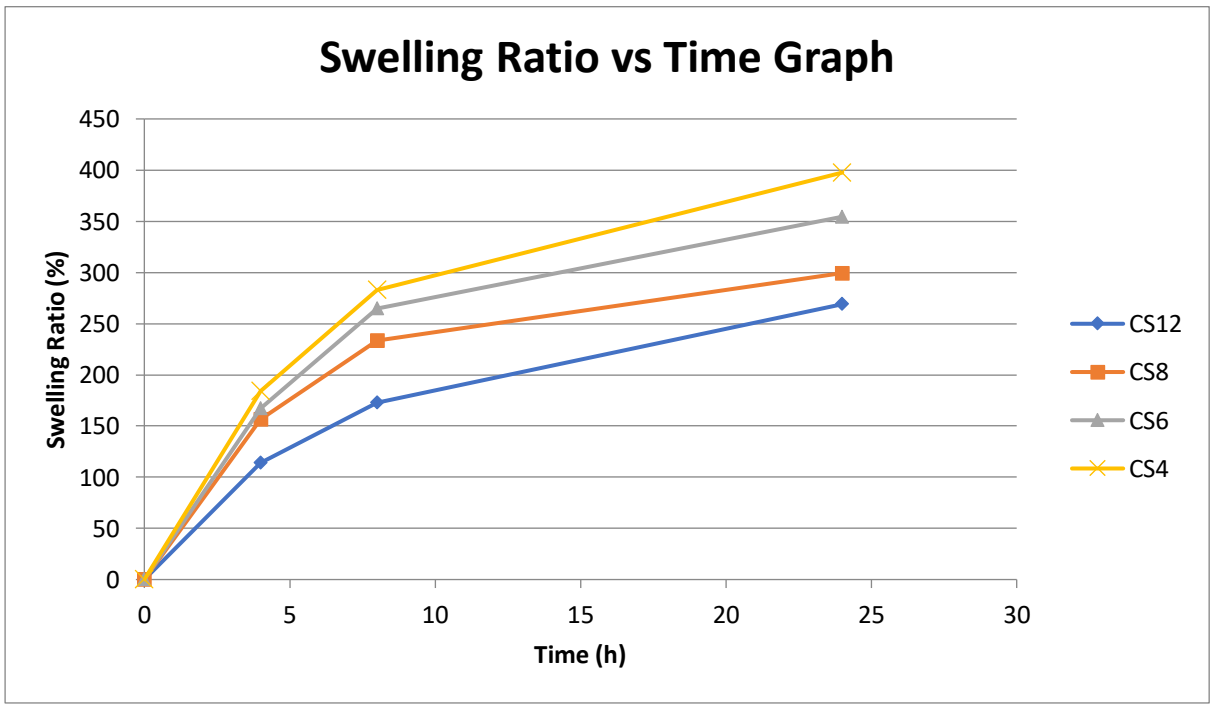

Figure 39: Swelling ratio graph.

Table 11: Results of swelling ratio test.

Hours	Swelling Ratios (%)			
	CS12	CS8	CS6	CS4
4	114	157.1	167.9	186.5
8	172.8	234.2	264.9	280.8
24	268.5	300	355.2	395.2

4) CONCLUSION AND DISCUSSION

The most common problem encountered in the use of electrospinning was the drying of the solution at the nozzle tip. If this problem is not resolved, dry particles will accumulate on the drum and the surfaces of the fibers will not be smooth. To solve this problem, the environment in which the production takes place should not be cold and should be humid.

The tensile tests for the fibers were performed using 2 different strain rates. These were 5mm/min and 30mm/min. High fluctuations were seen in the graphics at low strain rates. The reason for these high fluctuations is that some of the nanofibers in the sample break during testing and less force is applied due to the low strain rate.

According to Table 6, when boric acid nanoparticles were first introduced to fiber the elastic modulus decreases with respect to only PCL containing fiber. However, the elastic modulus of fibers containing a high boric acid percentage is higher than those containing low boric acid percentage. However, this increase is not sufficient. On the other hand, it was observed that the elastic modulus increased when the amount of ZnO increased. The highest ultimate tensile stress and elastic modulus values were observed in the fiber containing 10% ZnO. When the elongation percentages and graphic shapes were examined, it was observed that all fibers showed ductile properties. However, the fibers containing boric acid elongated more than those containing ZnO.

According to Tables 7 and 8, it was clearly seen that all fibers show hydrophobic properties. Nanoparticle addition has decreased the contact angle; however, they kept the hydrophobic behavior because contact angle values were never less than 90°.

Result of the compression tests of hydrogels, was listed in Table 10. It was clearly seen in this table that CS12 hydrogel has the highest strength. It was observed that when the amount of chitosan decreased and the amount of PVA increased the ultimate compressive stress also decreased. However, the ductility of the gel increased when PVA increased. To summarize, as the amount of chitosan increases, the material becomes more robust and brittle, and as the amount of PVA increases, the material becomes weaker and less brittle. Based on this result, it was concluded that PVA blocked the cross-linking of chitosan. This inference can be proved by the FTIR test results.

As a result of the swelling test for hydrogels, it was seen that by gradually decreasing the amount of chitosan in the hydrogel the swelling ratio increases. The reason for this

phenomenon was the crosslinking agent glutaraldehyde bonding with increasing amounts of chitosan, forming a denser and more intense structure thus leaving less space inside the hydrogel for water absorption. Contact angle test results also approve this phenomenon for the result of the swelling test.

5) FUTURE WORKS

To interpret the crosslinking effect and bond strength in hydrogels in more detail and precisely, the FTIR test should be performed. In this way, the amount of OH bonds can be examined in detail and the results can be interpreted more clearly.

In this project, the amount of glutaraldehyde contained in the hydrogels was kept constant. In future studies, the GA ratio can be increased, and the tests can be repeated at the same and different PVA ratios. Thus, it can be determined whether PVA blocks the crosslinking of chitosan.

The produced fibers and hydrogels can be stacked in different ways. A fiber mat in the top layer and hydrogel below or the top and middle layer is fiber mat, and for the inner(bottom) part of the dressing, where it is in contact with the wound, can be made more hydrophilic. Increasing the hydrophilicity of this layer can ease the absorption of the body fluid from the skin surface. More hydrophilic fiber mat can be used for this layer.

In our project, it was observed that as the ZnO ratio increased, the fiber mats became stronger. In future studies, fibers containing more than 10% ZnO can be produced and examined in order to find the optimum ZnO percentage.

REFERENCES

[1] Gozali, D., Hudaya, A. R., & Suharyani, I. (2022). A Review On Chitosan-Based Materials As Potential Wound Dressing Materials. In International Journal Of Applied Pharmaceutics (Pp. 27–32). Innovare Academic Sciences Pvt Ltd.

[2] Han, G., & Ceilley, R. (2017). Chronic Wound Healing: A Review of Current Management and Treatments. In Advances in Therapy (Vol. 34, Number 3, pp. 599–610). Springer Science and Business Media LLC.

[3] The Editors of Encyclopedia Britannica. (1998, July 20). Wound | Definition, Types, & Treatment. Encyclopedia Britannica. Retrieved February 14, 2023, from https://www.britannica.com/science/wound

[4] Wounds and Injures. Effective Health Care Program. (2018, November 27). Retrived February 15, 2023 https://effectivehealthcare.ahrq.gov/health-topics/wounds-and-injuries

[5] Younan, G. J., Heit, Y. I., Dastouri, P., Kekhia, H., Xing, W., Gurish, M. F., & Orgill, D. P. (2011). Mast Cells Are Required in the Proliferation and Remodeling Phases of Microdeformational Wound Therapy. In Plastic and Reconstructive Surgery (Vol. 128, Number 6, pp. 649e–658e). Ovid Technologies (Wolters Kluwer Health).

[6] Archana, D., Singh, B. K., Dutta, J., & Dutta, P. K. (2013). In vivo evaluation of chitosan–PVP–titanium dioxide nanocomposite as wound dressing material. In Carbohydrate Polymers (Vol. 95, Issue 1, pp. 530–539). Elsevier BV.

[7] Archana, D., Singh, B. K., Dutta, J., & Dutta, P. K. (2013). In vivo evaluation of chitosan–PVP–titanium dioxide nanocomposite as wound dressing material. In Carbohydrate Polymers (Vol. 95, Issue 1, pp. 530–539). Elsevier BV.

[8] Motasadizadeh, H., Azizi, S., Shaabani, A., Sarvestani, M. G., Sedghi, R., & Dinarvand, R. (2022). Development of PVA/Chitosan-g-Poly (N-vinyl imidazole)/TiO2/curcumin nanofibers as high-performance wound dressing. In Carbohydrate Polymers (Vol. 296, p. 119956). Elsevier BV.

[9] Teixeira, M. A., Paiva, M. C., Amorim, M. T. P., & Felgueiras, H. P. (2020). Electrospun Nanocomposites Containing Cellulose and Its Derivatives Modified with Specialized Biomolecules for an Enhanced Wound Healing. In Nanomaterials (Vol. 10, Number 3, p. 557). MDPI AG.

[10] Greiner, A., & Wendorff, J. H. (2007). Electrospinning: A Fascinating Method for the Preparation of Ultrathin Fibers. In Angewandte Chemie International Edition (Vol. 46, Number 30, pp. 5670–5703). Wiley.

[11] Ignatova, M., Rashkov, I., & Manolova, N. (2013). Drug-loaded electrospun materials in wound-dressing applications and in local cancer treatment. In Expert Opinion on Drug Delivery (Vol. 10, Number 4, pp. 469–483). Informa Healthcare.

[12] Murray, R. Z., West, Z. E., Cowin, A. J., & Farrugia, B. L. (2019). Development and use of biomaterials as wound healing therapies. In Burns & Trauma (Vol. 7). Oxford University Press (OUP).

[13] Aswathy, S. H., Narendrakumar, U., & Manjubala, I. (2020). Commercial hydrogels for biomedical applications. In Heliyon (Vol. 6, Number 4, p. e03719). Elsevier BV.

[14] Borda, L. J., Macquhae, F. E., & Kirsner, R. S. (2016). Wound Dressings: A Comprehensive Review. In Current Dermatology Reports (Vol. 5, Number 4, pp. 287–297). Springer Science and Business Media LLC.

[15] Kamoun, E. A., Kenawy, E.-R. S., & Chen, X. (2017). A review on polymeric hydrogel membranes for wound dressing applications: PVA-based hydrogel dressings. In Journal of Advanced Research (Vol. 8, Number 3, pp. 217–233). Elsevier BV.

[16] Jang, E. J., Patel, R., & Patel, M. (2023). Electrospinning Nanofibers as a Dressing to Treat Diabetic Wounds. In Pharmaceutics (Vol. 15, Number 4, p. 1144). MDPI AG.

[17] Xue, J., Wu, T., Dai, Y., & Xia, Y. (2019). Electrospinning and Electrospun Nanofibers: Methods, Materials, and Applications. In Chemical Reviews (Vol. 119, Number 8, pp. 5298–5415). American Chemical Society (ACS).

[18] Amariei, N., Manea, L. R., Bertea, A. P., Bertea, A., & Popa, A. (2017). The Influence of Polymer Solution on the Properties of Electrospun 3D Nanostructures. In IOP Conference Series: Materials Science and Engineering (Vol. 209, p. 012092). IOP Publishing.

[19] Mohammadzadehmoghadam, S., Dong, Y., & Jeffery Davies, I. (2015). Recent progress in electrospun nanofibers: Reinforcement effect and mechanical performance. In Journal of Polymer Science Part B: Polymer Physics (Vol. 53, Number 17, pp. 1171–1212). Wiley.

[20] Keshvardoostchokami, M., Majidi, S. S., Huo, P., Ramachandran, R., Chen, M., & Liu, B. (2020). Electrospun Nanofibers of Natural and Synthetic Polymers as Artificial Extracellular Matrix for Tissue Engineering. In Nanomaterials (Vol. 11, Number 1, p. 21). MDPI AG.

[21] Asmatulu, R. (2016). Highly Hydrophilic Electrospun Polyacrylonitrile/ Polyvinypyrrolidone Nanofibers Incorporated with Gentamicin as Filter Medium for Dam Water and Wastewater Treatment. In Journal of Membrane and Separation Technology (Vol. 5, Number 2, pp. 38–56). Lifescience Global.

[22] Özen, N., Özbaş, Z., İzbudak, B., Emik, S., Özkahraman, B., & Bal-Öztürk, A. (2021). Boric acid-impregnated silk fibroin/gelatin/hyaluronic acid-based films for improving the wound healing process. In Journal of Applied Polymer Science (Vol. 139, Number 9, p. 51715). Wiley.

[23] Rahmadiawan, D., Abral, H., Railis, R. M., Iby, I. C., Mahardika, M., Handayani, D., Natrana, K. D., Juliadmi, D., & Akbar, F. (2022). The Enhanced Moisture Absorption and Tensile Strength of PVA/Uncaria gambir Extract by Boric Acid as a Highly Moisture-Resistant, Anti-UV, and Strong Film for Food Packaging Applications. In Journal of Composites Science (Vol. 6, Number 11, p. 337). MDPI AG.

[24] Kapukaya, R., & Ciloglu, O. (2020). Treatment of chronic wounds with polyurethane sponges impregnated with boric acid particles: A randomised controlled trial. In International Wound Journal (Vol. 17, Number 5, pp. 1159–1165). Wiley.

[25] Etimaden Ürün Teknik Bilgi Formu Borik Asit. (2019, January). *Etimaden*. Retrieved February 17, 2023, from https://etimaden.gov.tr

[26] Lin, M., Liu, Y., Gao, J., Wang, D., Xia, D., Liang, C., Li, N., & Xu, R. (2022). Synergistic Effect of Co-Delivering Ciprofloxacin and Tetracycline Hydrochloride for Promoted Wound Healing by Utilizing Coaxial PCL/Gelatin Nanofiber Membrane. In International Journal of Molecular Sciences (Vol. 23, Number 3, p. 1895). MDPI AG.

[27] Yao, Q., Cosme, J. G. L., Xu, T., Miszuk, J. M., Picciani, P. H. S., Fong, H., & Sun, H. (2017). Three dimensional electrospun PCL/PLA blend nanofibrous scaffolds with significantly improved stem cells osteogenic differentiation and cranial bone formation. In Biomaterials (Vol. 115, pp. 115–127). Elsevier BV.

[28] Bakil, S. N. A., Kamal, H., Abdullah, H. Z., & Idris, M. I. (2020). Sodium alginate-zinc oxide nanocomposite film for antibacterial wound healing applications. Biointerface Research in Applied Chemistry, 10(6), 6289–6296.

[29] *Preguntas sobre el óxido de zinc*. (2015, February 10). Retrieved March 2, 2023, from https://ec.europa.eu/health/scientific_committees/opinions_layman/zinc-oxide/en/index.htm

[30] Barbarossa, G., & Barbarossa, G. (2021, October 29). Zinc Oxide Benefits and Wound Dressings - Hy-Tape International, Inc. *Hy-Tape International, Inc. - The Original Pink Tape. Zinc Oxide Waterproof Ostomy Wound Tape.* Retrieved March 4, 2023, from https://hytape.com/wound-care/zinc-oxide-benefits-and-wound-dressings/?v=920f83e594a1

[31] Teixeira-Costa, B. E., & Andrade, C. T. (2021). Chitosan as a Valuable Biomolecule from Seafood Industry Waste in the Design of Green Food Packaging. In Biomolecules (Vol. 11, Number 11, p. 1599). MDPI AG.

[32] Galed, G., Miralles, B., Panos, I., Santiago, A., & Heras, A. (2005). - Deacetylation And Depolymerization Reactions Of Chitin/Chitosan: Influence Of The Source Of Chitin. In Carbohydrate Polymers (Vol. 62, Number 4, Pp. 316–320). Elsevier Bv.

[33] Burkatovskaya, M., Tegos, G. P., Swietlik, E., Demidova, T. N., P Castano, A., & Hamblin, M. R. (2006). Use of chitosan bandage to prevent fatal infections developing from highly contaminated wounds in mice. In Biomaterials (Vol. 27, Number 22, pp. 4157–4164). Elsevier BV.

[34] Preparation of Chitosan-Polyvinyl Alcohol Blends and Studies on Thermal and Mechanical Properties AgilAbrahama , P.A.Solomanb ,V.O.Rejinib International Conference on Emerging Trends in Engineering, Science and Technology (ICETEST - 2015)

[35] Lu, Z., Gao, J., He, Q., Wu, J., Liang, D., Yang, H., & Chen, R. (2017). Enhanced antibacterial and wound healing activities of microporous chitosan-Ag/ZnO composite dressing. In Carbohydrate Polymers (Vol. 156, pp. 460–469). Elsevier BV.

[36] Madihally, S. V., & Matthew, H. W. T. (1999). Porous chitosan scaffolds for tissue engineering. In Biomaterials (Vol. 20, Number 12, pp. 1133–1142). Elsevier BV.

[37] Lee, D. W., Lim, C., Israelachvili, J. N., & Hwang, D. S. (2013). Strong Adhesion and Cohesion of Chitosan in Aqueous Solutions. In Langmuir (Vol. 29, Number 46, pp. 14222–14229). American Chemical Society (ACS).

[38] Matica, Aachmann, Tøndervik, Sletta, & Ostafe. (2019). Chitosan as a Wound Dressing Starting Material: Antimicrobial Properties and Mode of Action. In International Journal of Molecular Sciences (Vol. 20, Number 23, p. 5889). MDPI AG.

[39] Shrivastava, P., Vishwakarma, N., Gautam, L., & Vyas, S. P. (2023). Magnetically responsive polymeric gels and elastomeric system(s) for drug delivery. In Smart Polymeric Nano-Constructs in Drug Delivery (pp. 129–150). Elsevier.

[40] Firlar, I., Altunbek, M., McCarthy, C., Ramalingam, M., & Camci-Unal, G. (2022). Functional Hydrogels for Treatment of Chronic Wounds. In Gels (Vol. 8, Number 2, p. 127). MDPI AG.

[41] Francesko, A., Petkova, P., & Tzanov, T. (2019). Hydrogel Dressings for Advanced Wound Management. In Current Medicinal Chemistry (Vol. 25, Number 41, pp. 5782–5797). Bentham Science Publishers Ltd.

[42] Jones, A., & Vaughan, D. (2005). Hydrogel dressings in the management of a variety of wound types: A review. In Journal of Orthopaedic Nursing (Vol. 9, pp. S1–S11). Elsevier BV.

[43] Norioka, C., Inamoto, Y., Hajime, C., Kawamura, A., & Miyata, T. (2021). A universal method to easily design tough and stretchable hydrogels. In NPG Asia Materials (Vol. 13, Number 1). Springer Science and Business Media LLC.

[44] Xing, Q., Yates, K., Vogt, C., Qian, Z., Frost, M. C., & Zhao, F. (2014). Increasing Mechanical Strength of Gelatin Hydrogels by Divalent Metal Ion Removal. In Scientific Reports (Vol. 4, Number 1). Springer Science and Business Media LLC.

[45] Liu, H., Wang, C., Li, C., Qin, Y., Wang, Z., Yang, F., Li, Z., & Wang, J. (2018). A functional chitosan-based hydrogel as a wound dressing and drug delivery system in the treatment of wound healing. In RSC Advances (Vol. 8, Number 14, pp. 7533–7549). Royal Society of Chemistry (RSC).

[46] Isecke, B., Schütze, M., & Strehblow, H.-H. (2006). Corrosion In Springer Handbook of Materials Measurement Methods (pp. 611–684).

[47] Davis, J. R. (2004). Tensile Testing. ASM International.

[48] What is Tensile Testing? (n.d.). Retrieved March 9, 2023, from https://www.twi-global.com/technical-knowledge/faqs/what-is-tensile-testing

[49] Chellamuthu, Sabarinathan & Muthu, S. & Ali, M. (2012). Experimental study on tensile behavior of multi wall carbon nanotube reinforced epoxy composites. Journal of Applied Sciences Research. 8. 3253-3259

[50] Budynas, R. G. and Nisbett, J. K. (2011). Shigley's Mechanical Engineering Design, 9th edition ,McGraw-Hill, New York, USA

[51] *Modulus of Elasticity*. (n.d.). Instron. Retrieved April 12, 2023, from https://www.instron.com/en/resources/glossary/m/modulus-of-elasticity

[52] Main Takeaways on Stress and Strain. (n.d.). TuDelft. Retrieved April 23, 2023, from https://ocw.tudelft.nl/course-readings/1-1-6-main-takeaways-on-stress-and-strain/

[53] Brittle v ductile stress-strain behaviour.png - Wikipedia. (n.d.). Retrieved May 8, 2023, from https://tr.m.wikipedia.org/wiki/Dosya:Brittle_v_ductile_stress-strain_behaviour.png

[54] Chow, T. S. (1998). Wetting of rough surfaces. In Journal of Physics: Condensed Matter (Vol. 10, Number 27, pp. L445–L451). IOP Publishing.

[55] Susanna Laurén,(2021, May 11) Why should you use the water contact angle measurement instead of the water break test?. Retrieved May 16, 2023 from https://www.biolinscientific.com/blog/why-should-you-use-the-water-contact-angle-measurement-instead-of-the-water-break-test

[56] Semprebon, Ciro. (2009). Wetting on Anisotropically Patterned and Rough Surfaces.

[57] Centre for Industrial Rheology. (2023, March 16). Contact Angle Testing/Analysis - Rheology Lab. Rheology Lab. Retrieved May 16, 2023 from https://www.rheologylab.com/contact-angle/

[58] *What Is a Contact Angle?* (2022, April 7). Brighton Science. Retrieved May 23, 2023, from https://www.brighton-science.com/what-is-contact-angle

[59] Ahearne, M. & L., Kuo-Kang, I. (2008). Mechanical Characterisation of Hydrogels for Tissue Engineering Applications. Topics Tissue Eng. 4. Los Angeles, USA

[60] Ji, S., Zhao, Y., Zhai, X., Wang, L., Luo, H., Xu, Z., Dong, W., Wu, B., & Wei, W. (2023). A Dual-Crosslinked Hydrogel Based on Gelatin Methacryloyl and Sulfhydrylated Chitosan for Promoting Wound Healing. In International Journal of Molecular Sciences (Vol. 24, Number 3, p. 2447).

[61] Chua, C. K., Wong, C. H., & Yeong, W. Y. (2017). Benchmarking for Additive Manufacturing. In Standards, Quality Control, and Measurement Sciences in 3D Printing and Additive Manufacturing (pp. 181–212). Elsevier.

[62] Yahia, Lh. (2015). History and Applications of Hydrogels. In Journal of Biomedical Sciencies (Vol. 04, Number 02). OMICS Publishing Group.

[63] Sievers, J., Sperlich, K., Stahnke, T., Kreiner, C., Eickner, T., Martin, H., Guthoff, R. F., Schünemann, M., Bohn, S., & Stachs, O. (2020). Determination of hydrogel swelling factors by two established and a novel non-contact continuous method. In Journal of Applied Polymer Science (Vol. 138, Number 18, p. 50326). Wiley.

[64] *SOP - Tensile testing of electrospun nanofiber membrane*. (2013, July 3). ElectrospinTech. Retrieved May 29, 2023, from http://electrospintech.com/SOP-ES2002.html#.XIe4hR4xUwA

[65] Dong, F., & Li, S. (2018). Wound Dressings Based on Chitosan-Dialdehyde Cellulose Nanocrystals-Silver Nanoparticles: Mechanical Strength, Antibacterial Activity and Cytotoxicity. In Polymers (Vol. 10, Number 6, p. 673). MDPI AG.

[66] Standard Test Method for Tensile Properties of Thin Plastic Sheeting (ASTM D882-10)

[67] Chen, F., Peng, X., Li, T., Chen, S., Wu, X.-F., Reneker, D. H., & Hou, H. (2008). Mechanical characterization of single high-strength electrospun polyimide nanofibres. In Journal of Physics D: Applied Physics (Vol. 41, Number 2, p. 025308). IOP Publishing.

[68] Li, J., Liu, H., Wang, C., & Huang, G. (2017). A facile method to fabricate hybrid hydrogels with mechanical toughness using a novel multifunctional cross-linker. In RSC Advances (Vol. 7, Number 56, pp. 35311–35319). Royal Society of Chemistry (RSC).